Manuscript (Main plus SI text)
Click here to access/download;Manuscript;RAB11a paper Final.pdf

Zygote morphogenesis but not the establishment of cell polarity in *Plasmodium berghei* is controlled by the small GTPase, RAB11A

H. Patil†, K.R. Hughes†, L. Lemgruber, N. Philip, N. Dickens, A. P. Waters*

Wellcome Centre for Integrative Parasitology, Sir Graeme Davis Building, 120 University Place, University of Glasgow, Glasgow G12 8TA, Scotland, United Kingdom

* To whom correspondence should be addressed (Andy.Waters@glasgow.ac.uk)
ORCID ID: 0000-0001-8900-2982

† Contributed equally to the work.

Abstract

Plasmodium species are apicomplexan parasites whose zoites are polarized cells with a marked apical organisation where the organelles associated with host cell invasion and colonization reside. *Plasmodium* gametes mate in the mosquito midgut to form the spherical and presumed apolar zygote that morphs during the following 24 hours into a polarized, elongated and motile zoite form, the ookinete. Endocytosis-mediated protein transport is generally necessary for the establishment and maintenance of polarity in epithelial cells and neurons, and the small GTPase RAB11A is an important regulator of protein transport via recycling endosomes. PbRAB11A is essential in blood stage asexual of *Plasmodium*. Therefore, a promoter swap strategy was employed to down-regulate PbRAB11A expression in gametocytes and zygotes of the rodent malaria parasite, P. berghei which demonstrated the essential role of RAB11A in ookinete development. The approach revealed that lack of PbRAB11A had no effect on gamete production and fertility rates however, the zygote to ookinete transition was almost totally inhibited and transmission through the mosquito was prevented. Lack of PbRAB11A did not prevent meiosis and mitosis, nor the establishment of polarity as indicated by the correct formation and positioning of the Inner Membrane Complex (IMC) and apical complex. However, morphological maturation was prevented and parasites remained spherical and immotile and furthermore, they were impaired in the secretion and distribution of microneme cargo. The data are consistent with the previously proposed model of RAB11A endosome mediated delivery of plasma membrane in *T. gondii* and implicate it in microneme function.

Author Summary

According to the WHO there was estimated to be over 200 million cases of malaria in 2017 and nearly half a million deaths. The disease is caused by the Plasmodium parasite which is passed between human hosts by a mosquito vector. In order to transmit through the mosquito the single-celled parasite undergoes many developmental changes as it morphs from apolar and non-motile blood forms to polarised and motile ookinetes in the mosquito midgut. Transport of proteins within the cell during these critical transitions relies on specific endosome vesicles to correctly target proteins within the parasite. We investigated the role of the RAB11A protein which is known to be involved in endosomal vesicle targeting to generate cellular polarity in other organisms. Because RAB11A is also essential for parasite growth in the mammalian host we used a promoter swap system to specifically switch off the protein in the sexual transmission stages. In the absence of RAB11A parasites were unable to form elongated, motile ookinetes and were unable to pass through the mosquito. Interestingly the parasites were able to form some of the (polarising) structures specific to ookinetes however full morphological transformation did not occur and the parasites were not motile. We show that although proteins are still delivered to the parasite surface, secretion is impaired and that the mutant parasites are smaller despite obvious microtubule formation implying that there is a deficit in delivery of membrane to the surface.

Introduction

All zooites formed by apicomplexan parasites are polarized cells exhibiting an asymmetric distribution of content with defined apical distribution of the organelles (rhoptries and micronemes) involved in the recognition and colonisation of host cells. One of the early and critical events during mosquito transmission of malaria parasites (*Plasmodium* spp) is the initial development from (what is assumed to be) a non-polar zygote to a motile and polarized ookinete following fusion of a male and female gamete in the blood meal. This is essential for the parasite to be able to escape the hostile environment of the mosquito midgut and represents the greatest period of time that *Plasmodium* remains outwith a host cell. Although little is known about the generation of polarity in *Plasmodium* species, studies in other organisms have established that polarity is vital to carry out specific functions such as cell growth, migration, protein transport and invasion [1]. Indeed, all eukaryotes achieve cell polarity through a conserved set of proteins which includes signalling molecules of the *rho* family of GTPases, cytoskeleton assembly and recruitment, mobilization of proteins from the intracellular pool to the tip of growth via vesicle delivery [1]. Although, the *rho* family of GTPases such as Cdc42 and its homologues seem to be conserved in majority of organisms studied, there are species specific varieties of polarity determining proteins with little discernible general conservation [2]. The development and establishment of polarity can be regulated by internal factors such as protein trafficking, microtubules and actin dynamics [reviewed in [3]] and utilise both the exocytic and endocytic pathways to develop polarity [4]. The members of Ras GTPase subfamily are central to cell growth, differentiation and survival [reviewed in [5, 6]] and RAB proteins of which there are 11 in *Plasmodium* [7] belong to a small Ras GTPase family and regulate vesicle transport in eukaryotes.

RAB11A is involved in regulating vesicular traffic during recycling endosomes [8] and may assist in cytokinesis [9]. RAB11A is prenylated and interacts with phosphatidylinositol-4 kinases (PI4Ks) [10, 11] and its effectors such as RAB11A family of interacting proteins (FIPs)[12]. The role of RAB11A in apicomplexan parasites and *Plasmodium falciparum rab11a* (PF3D7_1320600) is essential [9] and it is expressed in all *Plasmodium* asexual blood stages with punctate protein localization in schizonts [7, 11]; [13] that by analogy with *T. gondii* may be an association with rhoptries [14]; [9]. *T. gondii* expressing ddFKBP-Rab11A dominant negative form (ddFKBP-Rab11A$_{DN}$) shows reduced invasion of host cells by ~85%, consistent with a role in transport and release of rhoptry content during invasion [15]. Furthermore, preceding schizogony, co-localization studies of GAP45 and RAB11A support the notion that RAB11A also mediates the delivery of GAP45 to the Inner Membrane Complex (IMC) and interacts with elements of the motility apparatus Microtubule Interacting Protein/Myosin Light chain (MTIP/MLC) but plays no role in the organelle biogenesis and localization of sub-pellicular

microtubules [9]. However, in *T. gondii*, the correct delivery of the major surface antigen SAG-1 to the plasma membrane requires functional RAB11A as the ddFKBP-Rab11A$_{DN}$ line showed patchy (abnormal) instead of smooth (normal) localization of SAG1 [9]. RAB11A controls the necessary step after biogenesis of secretary organelles but before assembly of the motor complex during cell division. These data suggest that RAB11A along with unconventional myosin controls the IMC assembly and budding of daughter cells. *Plasmodium* iterates the formation of zoites through its life cycle with their attendant features of an IMC and apical organelle formation raising the prospect that the roles of RAB11A might be also be reiterated. Indeed, the transcript encoding PbRAB11A is one of 370 transcripts which are stabilized and translationally repressed by the DOZI translational repression complex in gametocytes of the rodent infectious malaria model, *Plasmodium berghei* [16, 17], indicating its potential role in ookinete development. Therefore, further investigation of PbRAB11A function in the fertilised female gamete (zygote) may reveal insights into the development of polarity in ookinetes, in *P. bergh*ei.

Here, using a promoter swap strategy we show that PbRAB11A is essential for the transmission of *Plasmodium* through mosquitoes. Lack of PbRAB11A in ookinetes does not affect the formation of internal, polarised landmarks such as the apical complex and IMC in developing zygotes: meiosis and translation of stored mRNAs is also achieved. However, chromosomes remain decondensed 24 hours post fertilization and zygotes are morphologically arrested and remain spherical. These data suggested that PbRAB11A has no role in the establishment or development of zygote polarity in *P. berghei* and instead is necessary for morphological progression in a manner consistent with the model of PbRAB11A mediated delivery of plasma membrane proposed for daughter cell formation in *T. gondii* tachyzoites and *Plasmodium* asexual blood stage forms.

Results

PbRAB11A is expressed throughout *P. berghei* life cycle and localizes to the periphery and apical tip of the ookinete.

The protein encoded by *pbrab11A* (PBANKA_1418900) is expressed in all stages of the *P. berghei* life cycle examined and most abundant in gametocytes [13] (Fig 1A). A polyclonal antibody raised against the C-terminal end of PBRab11A was used in Western analysis of the WT-GFP$_{CON}$, [18] line and demonstrated expression of *pbrab11a* across mixed asexual stages, schizonts, gametocytes and ookinetes. A smaller, ~23kDa band of unknown significance was detected indicating possible differential regulation or N-terminal processing of PbRAB11A in schizonts and mature ookinetes (asterisked in Fig 1. B, C). Immunofluorescence microscopy using the same polyclonal antibody on fixed in WT-GFP$_{CON}$, parasites showed expression of PbRAB11A in mature schizonts (individual merozoites), 6h zygotes, ookinetes, oocysts as well as midgut sporozoites (Fig 1D). In merozoites, oocysts (day10) and midgut sporozoites (day10), the localization of PbRAB11A appears to be cytoplasmic. In the 6h zygote, PbRAB11A is cytoplasmic and appears punctate while in the ookinete PbRAB11A is more peripheral and with a focus at the apical tip suggesting a role of PbRAB11A at the apical complex (Fig 1D).

Rab11A is necessary to generate normal ookinete morphology, motility and for transmission.

The essential nature of PBRAB11A in the asexual blood stages [9] required a conditional approach for gene disruption to study protein function in the ookinete stage. The promoter swap strategy that has been previously validated [13, 19, 20] remains the most reliable method to knock down gene expression during the gametocyte to ookinete transition especially where modification of the protein of interest at the C-terminus would inactivate the protein. Both *clag* (PBANKA_140060) and *ama-1* (PBANKA_091500) promoters are known to remain silent in sexual stages whilst maintaining sufficient expression levels during asexual blood stages [13, 19, 20]. The 0.9 kb 5'UTR of *rab11a* was replaced by 2 kb 5'UTR of *clag* (referred to as $_p$*clag*) or 1.7 kb 5'UTR of *ama-1* (referred to as $_p$*ama-1*) and a *2cmyc* N-terminal tag using conventional single crossover homologous recombination in WT-GFP parasites which were selected and cloned via serial dilution [21]. Both independently generated *pbab11A* promoter-swap mutants: $_p$*clag:2cmyc::rab11a* and $_p$*ama-1:2cmyc::rab11a* (henceforth referred as $_p$*clag::rab11a* and $_p$*ama-1::rab11a*) show appropriate genomic integration of the introduced constructs (Fig S1).

The two independently generated *pbab11A* promoter-swap mutants: $_p$*clag::rab11a* and $_p$*ama-1::rab11a* show no apparent growth defects during blood stages and gametocytogenesis (analysed by morphological comparison of gametocytes, exflagellation of male gametocytes, ratio of male to female gametocytes in parasites (Fig S2). However, visual inspection of *in vitro* ookinete cultures of $_p$*clag::rab11a* and $_p$*ama-1::rab11a* parasites revealed a severely impaired zygote to ookinete development by up to 99% and 98%

respectively (Fig 2A-C). Zygotes of both promoter swap lines remained spherical and failed to develop the characteristic elongated morphology of a wild type ookinete although the mature ookinete surface marker p25 was expressed and distributed to the surface of both promoter swap lines (Fig 2A-C). Western analysis of $_p$*clag::rab11a* and $_p$*ama-1::rab11a* show normal expression of RAB11A in mixed asexual blood stages, however, PbRAB11A is down-regulated in $_p$*clag::rab11a* and $_p$*ama-1::rab11a* gametocytes and ookinetes (Fig 2D, E). The additional smaller form of PbRAB11A noted in schizonts and mature ookinetes was only detected by the polyclonal PbRAB11A antisera and not by the anti c-myc antibody indicating that the protein confirming that the smaller isoform lacks the N-terminus of the larger form and therefore the c-myc epitope that would be present in the promoter swap lines. The $_p$*clag::rab11a* line was arbitrarily chosen for further analysis and western analysis demonstrated that its zygotes failed to produce significant levels of PbRAB11A from 2-24hpa (hours post activation) (Fig 2B, D, E,). Immunofluorescence studies support the down-regulation of PbRAB11A in $_p$*clag::rab11a* "ookinetes" (Fig 2B). The expression of the paralogous RAB11B in $_p$*clag::rab11a* was unaffected during zygote to ookinete development (Fig S3). Activated-Unfertilized 24h WT-GFP Female Gametes (AUFG - treated prior to and during activation with 2-Deoxy-D-glucose, 2DG [22] show expression of PbRAB11A and p25 (Fig 2B, E) indicating activation of translationally stored mRNAs occurred and was not dependent upon fertilisation (Fig S3). An imaging flow cytometry (IFC) strategy (Fig S4, S5) was developed to quantitate the ookinete conversion rate and confirmed the results seen by conventional microscopy (Fig 2F). Using IFC the level of the P25 on the parasite surface was also measured and compared to the degree of ookinete development. This showed that P25, although still strongly expressed was expressed at slightly lower levels in the promoter swap lines compared to the control line (Fig 2G). IFC was also used to measure the perimeter of the parasite as a measure of the surface area of parasites. Mature elongated wild type ookinetes as expected had an increased perimeter measurement and the predominantly circular parasites of the promoter swap lines retained a lower perimeter measurement similar to immature zygotes and are therefore of smaller surface area (Fig 2H). The $_p$*clag::rab11a* zygotes were able to complete meiosis (Fig S6) and both male and female *rab11a* alleles appear to contribute to the full development of the ookinete since crosses with P47ko and P48/45 ko lines which make competent male or female gametes respectively only partially restore the ability to generate wild type numbers of mature, morphologically normal ookinetes (Fig S7). The nucleus of the $_p$*clag::rab11a* "ookinetes" appears decondensed suggesting a qualitative impact on DNA replication (Fig S7).

To determine if the mainly spherical $_p$*clag::rab11a* and $_p$*ama-1::rab11a* ookinete populations were able to complete the life cycle through their invertebrate host, mosquito transmission experiments were performed (Fig 3). Female *Anopheles stephensi* mosquitoes were allowed to feed on WT-GFP$_{con}$, $_p$*clag::rab11a* or $_p$*ama-1::rab11a* infected mice. Mosquito midguts were examined for the presence of oocysts on day 11 or 14. Mosquito midguts were also analysed on day 17, 18 or 22 assuming that

$_p$clag::rab11a and *$_p$ama-1::rab11a* spherical ookinetes might have delayed midgut transversal and oocyst development. The WT-GFP showed normal oocyst development in mosquito midguts [median 150, mean 227 oocysts per midgut (n=3)] while *$_p$clag::rab11a* (maximum of 4 oocysts per midgut with small size, mean 0.269, median 0 and n=3) (Fig 3A, B) or *$_p$ama-1::rab11a* (maximum of 5 oocysts per midgut with small size, mean 0.31, median 0, n=2) (independent WT-GFP control for *$_p$ama-1::rab11a* showed mean 84, median 130.47, n=2) showed greatly reduced numbers of oocysts and salivary gland analysis showed a complete absence of *$_p$clag::rab11a* and *$_p$ama-1::rab11a* sporozoites (Fig S8). Upon feeding of infected mosquitoes on mice (bite-back) on day 18, 22 or 24, no parasites were observed in *$_p$clag::rab11a* (n=3) or *$_p$ama-1::rab11a* (n=2) infected mice which were monitored until day 14 post infection while WT-GFP parasites were observed on day 3 in all experiments (Table S1 and S2). Therefore, PbRAB11A is essential for the transmission of *P. berghei* and its role in the generation of ookinete morphology appears critical.
Due to the inability of *$_p$clag::rab11a* ookinetes to infect mosquito midguts and their spherical shape, the motility of *$_p$clag::rab11a* spherical ookinetes was examined in a comparative assay. 24hpa WT-mCherry and GFP-positive *$_p$clag::rab11a* zygotes (i.e. ookinetes) were embedded in the same Matrigel preparation (see Materials and Methods) and their motility observed in the red and green fluorescent channels. WT-mCherry ookinetes possessed normal corkscrew like movement and an average speed of ~10 µm/min whereas *$_p$clag::rab11a* spherical ookinetes were completely immobile (n=2) (Fig 3 C, D, Supplementary Video 1). This indicates that *$_p$clag::rab11a* ookinetes are immobile either due to the spherical morphology caused by lack of PbRAB11A and/or possible lack of motility associated proteins and therefore, transmission through mosquitoes is blocked.

PbRAB11A is not necessary for the generation and deposition of the apical complex and the IMC.

The demonstration that PbRAB11A production is necessary for the generation of ookinete, morphology, motility and infectivity prompted a further examination of the mutant parasite ultrastructure using electron microscopy. Scanning electron microscopy (SEM) demonstrated that 8h WT-GFP zygotes have progressed to the retort form while 8h *$_p$clag::rab11a* zygotes have a small outgrowth of plasma membrane possibly indicating a site for apical complex development (yellow arrow, Fig 4A). Transmission electron microscopy (TEM) of the same samples demonstrated that the IMC had been fully developed as well as the apical complex in 8h *$_p$clag::rab11a* zygotes with readily identifiable Apical Ring (APR) with an aperture (Ap), micronemes (M), Inner membrane complex (IMC) and subpellicular microtubules (Mt) (Fig 4B). EM imaging of parasites after 24 hours of development showed the development of the *$_p$clag::rab11a* zygotes has barely progressed whereas the WT-GFP parasites exhibited the expected, fully elongated form of mature ookinete (Fig 4C, D). This suggested that a full (and functional) apical complex was developed by *$_p$clag::rab11a* zygotes consisting of the IMC and internal organelles (see below) somewhat in contrast to the role for RAB11A in the delivery of surface and IMC markers in T. gondii [9].

The expression and distribution of a number IMC and apical organelle components by developing *pclag::rab11a* zygotes for which antibody reagents were available was, therefore, examined both by Western blot analysis and where possible immunofluorescence, comparing them to wild type parasites or activated unfertilised female gametes (AUFG) as controls. Western analysis of glideosome associated proteins: MTIP, GAP45 and GAP50, MyoA suggested a possible marginal delay in their expression between 6 to 8hpa and overall reduction in protein expression in *pclag::rab11a* zygotes (Fig 5A). Similarly, the expression of ookinete secreted or surface distributed proteins (chitinase and P28) appeared to be delayed and/or reduced (Fig 5A). The expression of cytoplasmic and more general structural proteins seemed unaffected (DOZI, CITH and alpha-tubulin). The expression of a protein known to be associated with the apical tip of the developing ookinete, the protein phosphatase PPKL seems unaffected in the *pclag::rab11a* line consistent with the observations that the apical complex is established as normal in the absence of PbRAB11A (Fig 5A, S9).

Immunofluorescence microscopy revealed that all IMC (GAP45, GAP50, IMCb, MTIP, MyoA), invasive organelle (Chitinase, CTRP) and surface markers (P25) appear to be distributed where expected within the spherical mutant *pclag::rab11a* matured zygotes (Fig 5, S9). In addition, PPKL serves as a marker for the apical tip of the mature ookinete and occupies a similar discrete location in *pclag::rab11a* matured zygotes alongside evident microtubule formation (Fig. S9). Furthermore, the localised dynamics of IMC protein deposition seemed similar despite the morphological differences between the ookinetes. The localization of GAP45 in *pclag::rab11a* zygotes was similar at 4h post-fertilization to WT-GFP, which indicates an initial focal point or bud development site from which the leading apical end will emerge (Fig S10) However, although *pclag::rab11a* 6h zygotes lack a prominent retort outgrowth, GAP45 is deposited in this mutant along the IMC showing an arc-like localization and apparently bordering the whole IMC at 24h post fertilization (Fig 5B). The IMC is linked to the subpellicular microtubule network that is critical for parasite motility and morphology. To further investigate the development of this tubulin-based structure we used a live-cell permeant tubulin stain to perform IFC analysis on live parasites at different stages of development. Analysis of live parasites showed that activating male gametocytes and male gametes could be clearly visualised and the intensity and distribution of tubulin was unchanged in the Rab11A- lines compared to the control (Fig 5C, D). At 4 hpa activated females identified by their P25 surface marker showed a discrete focus of tubulin stain representing the formation of the apical complex and site for outgrowth during subsequent parasite development (Fig 5E). This point was clearly present in both WT and mutant parasites, again suggesting that Rab11A is not essential for defining polarity in developing ookinetes. By 24 hpa the tubulin stain was unable to permeate through the membrane of live ookinetes but following partial permeabilisation using L-α-Lysophosphatidylcholine (LysoPC) we were able to visualise the tubulin based cytoskeletal structure in some mature live ookinetes. The promoter swap mutant lines showed tubulin staining around the parasite (Fig 5F) again showing similar intensity and

distribution around the periphery of the incompletely formed "ookinetes" compared to WT control ookinetes.

In order to assess possible transcriptional consequences linked to the morphological defects, RNA-seq analysis was performed on both gametocytes and cells resulting from 24 hour cultures of activated gametocytes that would normally generate ookinetes using wild type and $_p$*clag::rab11a* parasites. Little transcriptional effect was noted in gametocytes (9 transcripts upregulated more than 2-fold and 49 similarly downregulated, Fig S11) and there was no significant overlap of the de-regulated transcripts with the pool of transcripts that are destabilised in the absence of CITH or DOZI (1 transcript encoding a conserved protein of unknown function, PBANKA_0707700, Fig. S12). GO-term analysis did not reveal functional classes of transcript that were affected by the absence of PbRAB11A. There was a slightly stronger effect on ookinete transcription reflected in the number of transcripts with altered steady state level (32 downregulated, 84 upregulated, Fig S13).

In the absence of obviously significant differences in protein expression, deposition and transcription, furthermore taking into account of the expected role of PbRAB11A in microneme biogenesis, we examined the functionality of secretion from the apical organelles which is known to be important for the progressive surface distribution of motility associated proteins (e.g. CTRP) and soluble enzymes associated with life cycle progression (e.g. chitinase) (reviewed in [23]. Using CTRP and chitinase as the markers for the two fates of apical organelle cargo we compared relative amounts produced by wt and the two mutant $_p$*clag::rab11a* and $_p$*ama1::rab11a* parasites after 24 hours of culture of activated gametocytes when mature ookinetes would normally be present. We compared levels of parasite-associated protein in gently pelleted parasites and amounts released into the culture supernatant using a soluble non-secreted cytoplasmic protein (DOZI) as a marker for parasite lysis and normalisation. Reduced production of both chitinase and CTRP was evident in both mutants as well as significantly reduced chitinase secretion (Fig 6).

Discussion

Obligate intracellular protozoan parasites such as those represented by the Apicomplexa are likely to have further evolved the endocytic pathway common to all eukaryotes to suit the specialised needs of their intracellular niche. RAB11A is a highly conserved protein that can serve as a marker of both regulated and constitutive secretory pathways that may also ultimately deliver proteins to the host cell surface [24]. *Plasmodium* spp. also have an extended period where they exist as an extracellular parasite in the blood meal of the mosquito following gamete formation during the development of the zygote to form the motile ookinete that will subsequently encyst at the basolaminar side of the mosquito midgut. This extracellular phase of the life cycle offers an opportunity to study the development of a stable, polarised apicomplexan cell without the influence of a surrounding host cell. Secretory activities (including those involving PbRAB11A) will be confined to the delivery of membrane bound or secretory proteins to the parasite cell surface or to the specialised organelles associated with ookinete invasion (micronemes) for subsequent programmed release.

Previous attempts to delete PbRAB11A in haploid blood stages of *P. berghei* were unsuccessful indicating essentiality [9]. The abundance of *rab11A* mRNA in gametocytes [13] and the expectation that this mRNA was translationally repressed [16] suggested a role for PbRAB11A in ookinete development. We employed a c-MYC N-terminal tagging and a promoter swap strategy [19, 20] in order to avoid alteration of the C-terminus which contains a highly conserved and essential pair of cysteine residues necessary for the conserved geranylgeranylation required for RAB11A function ([25];[26]). Two independent mutant parasite lines: *pclag::rab11a* (G480) and $_p$*ama-1:rab11a* (G481) exploiting the late schizont *clag* and *ama-1* promoters respectively, were shown to facilitate the blood stage asexual expression of PbRAB11A to normal levels and showed no obvious growth defect. However, *rab11a* was effectively silenced in the sexual stages allowing examination of protein function during gametocyte and zygote development. Our results also extended the analysis of the expression of PbRAB11A during the *P. berghei* lifecycle (Figs 1 & 2) with Western analysis suggesting that two isoforms of PbRAB11A are produced in schizonts and ookinetes due to N-terminal processing. However, the significance of the observation is unclear and requires further investigation.

The absence of PbRAB11A in the $_p$*clag::rab11a* and $_p$*ama-1::rab11a* lines resulted in the formation of spherical ookinetes with an intact apical complex and IMC. Transcription and translation were also shown largely to be uncoupled to cellular development as both protein and transcriptome analyses revealed no striking differences from wild type gametocytes and ookinetes. Similarly spherical (and developmentally arrested) ookinetes of *P. berghei* were observed when *gap45* [27] and *pdeδ* [28] KO lines were analysed. However, the similarities are superficial given that GAP45 is expressed with only a slight delay and the IMC is correctly anchored in the *pclag::rab11a* spherical ookinetes unlike in the *gap45*$^-$ equivalents where the apical complex was observed to float freely inside the cytoplasm [27]. GAP45 is believed to be

delivered to the IMC by Rab11A-mediated vesicles [9] and is also responsible for retort formation [27]. Localization studies of GAP45 suggest the selection of a focal point in *pclag::rab11a* 4h zygotes which then disperses along the membrane of *pclag::rab11a* 6h zygotes lacking the WT retort outgrowth and lays down the IMC across the entire cytoplasmic side of the plasma membrane of the spherical *pclag::rab11a* ookinete (24hpa) indicating the assembly of IMC (Fig S10 and Fig 5 B). Our data, however, suggest that delivery of GAP45 does not depend on PbRAB11A mediated vesicles at this stage of parasite development. Equally in ddFKBP-Rab11A$_{DN}$ tachyzoites expressing a dominant negative form of TgRAB11 the membrane surface protein, SAG1 was not delivered correctly to the cell surface [9] yet delivery of an equivalent surface marker in the developing Plasmodium zygote, P25, seems unaffected and smoothly decorates the surface.

SEM analysis revealed a small, cone-like outgrowth in 8h *pclag::rab11a* zygotes (Fig 4 A). Analysis of 8h *pclag::rab11a* zygotes strongly suggest the outgrowth is associated with the assembly of the collar with an aperture, apical microtubules and the IMC (Fig 4 A, B). Therefore, assembly of complete set of internal organelles such as IMC, apical complex and micronemes is expected in spherical *pclag::rab11a* ookinetes and is somewhat comparable with the morphology of round dedifferentiated PDEδ KO *P. berghei* ookinetes which although they also form apical organelles, possess an incomplete IMC [28]. These round otherwise terminally differentiated PDEδ KO *P. berghei* ookinetes were shown to rotate rapidly but have little or no forward motility. The same motility assays suggest that *pclag::rab11a* spherical ookinetes do not exhibit even rotational movement (Fig 3 C, D) indicating a distinct developmental lesion. ImageStream analysis of *pclag::rab11a* "ookinetes" indicated that these cells had a smaller surface area than the wt ookinete equivalents and were therefore smaller. A recent study investigating delayed death phenotype in apicomplexan parasites has implicated a prenylation dependent role for RAB11A in the delivery of vesicular cargo (including GAP450) and intracellular trafficking [29]. Our data would be consistent with a deficit in delivery of lipid to the surface due to the absence of RAB11a implying there is also a stage specificity to the role of RAB11A and its cargo.

Spindle microtubule number varies greatly in the different zooite forms of *Plasmodium* (summarised in [30]) with ookinetes typically expressing around 60 [31] [32], merozoites 3-4 [33] and P. berghei sporozoites 16 [30]. The failure of our rab11A mutant retorts to fully elongate might indicate that there was an uncoupling of the IMC from the spindle microtubules. Direct investigation of this using tubulin tracker in live zygotes/ookinetes and SEM analysis of fixed samples demonstrated an early event at 4hpa visualised as a single centre of polarised nucleation of tubulin subtending the plasma membrane. Unfortunately, ookinetes become impermeable and live tracking of the microtubule development and organisation is not possible. Although SEM evidence was inconclusive it did demonstrate a regular array of microtubule origins around the apical prominence. Furthermore, immune-staining of tubulin indicated that microtubules are formed in parasites in the absence of RAB11A. Microtubule length can be a function

of type and levels of expression [30], however, there was no apparent impact of lack of RAB11A on tubulin abundance. Despite the abundance of microtubules in the ookinete the function of RAB11A does not appear to involve microtubule formation.

Although no major perturbances in transcription profile were detected in the *pclag::rab11a* gametocytes and ookinete forms, there was a minor temporal delay in protein expression of certain proteins assayed with our panel of antibodies. Furthermore, the expression of microneme proteins CTRP (also associated with ookinete motility) and chitinase appears to be reduced in *pclag::rab11a* and *pama1::rab11a* ookinetes than WT-GFP ookinetes although micronemes are clearly formed (Fig 4 D). Secretion assays confirmed the reduced expression of CTRP and chitinase and demonstrated that there was no obvious secretion of chitinase indicating functional impairment of apical organelle secretion. A deficiency in secretion is also supported by the immunofluorescence data which indicate that both CTRP and chitinase localise in a pattern consistent with deposition in the apical organelles.

Based on current results and past studies, we propose a model for developmental block of *pclag::rab11a* spherical ookinetes (Fig 7). The essential apical marker ISP1 is polarised in late female zygote indicating pre-selection of the focal point of ookinete [34]. Published data [27] and our results (Fig. 5, S10) suggest that GAP45 is also important for further development of the focal point, however, our data demonstrate that along with GAP45, PbRAB11A is critical for the retort outgrowth of *P. berghei* zygote. Once the focal point is marked through ISP1, GAP45 might start assembling at the focal point 4h post-fertilization along with as yet unknown focal point markers but which might include components of the IMC, collar and MTOC [35-37] through which microtubules extend. Subsequently, PbRAB11A along with cytoskeletal components such as actin as well as microtubules assist in the retort shape formation. Specifically, PbRAB11A endosomes might provide plasma membrane to the growing tip or to the joint of the retort and the main body of the zygote (here we refer to it as the 'neck' region) (Fig 7) and anticipate a role for Rab11A in the secretion, delivery of membrane synthesis components e.g. PI4K [11] and other necessary proteins while donating plasma membrane to assist the intended morphological transformation. Along with plasma membrane, the PbRAB11A endosome might help directly or indirectly in the incorporation of marker(s) at the neck region forming a transition point segregating the initial spherical body of the zygote from the retort outgrowth. Forces might be generated at the transition point that pushes the growing apical complex outwards by donating plasma membrane. Furthermore, the transition point 'neck marker/s' may act as a centre for pulling the plasma membrane during ookinete development. In *pclag::rab11a* zygotes, all characterised developmental and structural markers are formed normally however, we hypothesise that due to a lack of PbRAB11A mediated endosomes no plasma membrane is

made available for the growing apical complex and/or neck markers are probably mis-localized ultimately permitting apical bud formation but not outgrowth.

The zygote developmental processes described here serve as models for the developmental events of intracellular forms of *Plasmodium* such as sporozoites and merozoites as well as other apicomplexans that might be exploited for disease interventions. Our data highlight, however, that there may well be stage and species-specific features to even these essential processes.

Materials and Methods

Animal procedures and parasite reference line

Parasites were maintained in Theiler's original (TO) or NIH Swiss outbred female mice, approximately weighing 25 g and > 6 weeks old. All animal work was approved by the University of Glasgow's Animal Welfare and Ethical Review Body and by the UK's Home Office (PPL 60/4443). The animal care and use protocol complied with the UK Animals (Scientific Procedures) Act 1986 as amended in 2012 and with European Directive 2010/63/EU on the Protection of Animals Used for Scientific Purposes. The baseline used in all experiments was wildtype (WT) *P berghei* strain HPTBB or WT-GFP line [18].

Generation of mutant parasites

All the genes, 5'UTRs and 3'UTRs amplifications were performed using either Expand high fidelity PCR system (Roche) or KAPA HiFi PCR system (KAPA Biosciences) and diagnostic PCRs were performed using Taq DNA polymerase (Invitrogen) as per manufacturer's instructions.

3'UTR of *the snare* (PBANKA_141880) was amplified from gDNA of WT *P berghei* by using forward primer GU1620 and reverse primer GU1621 (Table S3) and re-cloned into pG72 (Dr. L. Starnes-Waters Group unpublished) to generate $_{p}$*clag:2cmyc::rab11a* construct ('$_{p}$' stands for promoter). Construct $_{p}$*ama-1:2cmyc::rab11a* was obtained by replacing *clag* 5'UTR in $_{p}$*clag:2cmyc::rab11a* with PCR amplified 1.7 Kb 5'UTR of *ama-1* (PBANKA_091500) ORF from gDNA of WT *P. berghei* using forward primer GU1622 and reverse primer GU1623 (Table S3). Plasmids $_{p}$*clag:2cmyc::rab11a* and $_{p}$*ama-1:2cmyc::rab11a* were verified by restriction digestion as well as Sanger sequencing (Eurofins MWG biotech). Purified and *HindIII-NotI* (New England Biolabs) linearised genomic constructs were obtained by gel extraction (QIAquick Gel Extration Kit) and subsequent ethanol precipitation. >5µg of linearized genomic constructs were transfected into WT-GFP *P. berghei* [18] schizonts as described in [21] and [38] to express PbRab11A under the control of either *clag* (PBANKA_140060) or *ama*-1 promoter respectively. (**Note:** $_{p}$*clag:2cmyc::rab11a* and $_{p}$*ama-1:2cmyc::rab11a* were referred as $_{p}$*clag::rab11a* and $_{p}$*ama-1::rab11a* throughout respectively.)

Plasmodium berghei infections, cultures and stage enrichment

Mice were infected by *intraperitoneal (i.p.)* injection either by fresh infected blood with PBS or by approximately 200µl of blood suspension having parasitaemia 3-5% from thawed cryovials. Post-infection mice develop parasitaemia approximately 0.5-3% on day 3, and for some experiments, mice were given a single dose of 100 µl phenylhydrazine (12.5 mg/ml) (mice bodyweight ratio 125mg/kg) *i.p.* to enhance numbers of reticulocytes usually 48 h prior infection. Parasitaemia was monitored daily by Giemsa staining

of thin smears of mouse tail blood [21] and parasites were observed under oil immersion (Invitrogen) 100x objective of light microscope (Primo Star- Zeiss). Images were captured through PAXcam5 camera using PAXcam software and processed using Fiji/ImageJ software (National Institute of Health, http://fiji.sc/Fiji).

Schizonts were generated as described in [21]. For enrichment of gametocytes, post 72 h of infection mice were treated with sulfadiazine (30 mg/litre) in drinking water for 48h to kill asexual parasite stages. For ookinete cultures, cardiac blood containing gametocytes was placed into ookinete culture medium (RPMI1640 containing 25 mM HEPES, 5 mM hypoxanthine, 20% FCS, 10 mM sodium bicarbonate, 100 µM xanthurenic acid at pH 7.6) and incubated at 21°C for 24h. Schizonts, gametocytes and ookinete development was observed by Giemsa staining. Ookinete conversion rates were calculated either from Giemsa staining or immunofluorescence microscopy using Cyanine3-tagged anti-P25 antibody (see immunofluorescence assay methods) of ookinete culture. Ookinete conversion rates were calculated according to the following formula:

$$\%\ ookinete\ conversion = \left(\frac{number\ of\ ookinetes\ analysed\ through\ morphology}{number\ of\ ookinetes\ + number\ of\ female\ or\ zygotes}\right)$$

To analyse activation centres cardiac blood was placed immediately into ookinete culture medium (1:30 blood to ookinete medium ratio) and 10 µl was placed on a haemocytometer at 21°C. After 15 minutes, activation centres defined as actively moving clumps of cells were counted using 10X objective on the light microscope (Primo Star- Zeiss). Fertility of mutant gametes was assessed through *in-vitro* cross fertilization with *P. berghei* parasites able to produce only male (P47 KO) [39] or female (P48/45 KO) gametes [40], respectively, by inhibiting mutant male gamete exflagellation through 2DG treatment [22].

Transmission

Transmission of parasites was performed by feeding 200 or 300 *Anophelese stephensi* mosquitoes on anaesthetized infected mice having 2-8% parasitaemia. Mosquitoes were dissected on day 11 or 14 post-feeding for oocyst counting and on day 17, 18 and 22, 27 post-feeding for oocysts and sporozoite counting. Midguts and salivary glands were examined with Leica M205 FA Fluorescence Stereomicroscope and images were captured using Leica DFC340FX camera and through LAS AF Lite 2.2.0 build 4758 (Leica Microsystems Ltd.) and processed through ImageJ/Fiji software (National Institute of Health). Oocyst numbers were counted by live imaging.

Motility assay

MACS-purified ookinetes were embedded in Matrigel and incubated for 1h at 21^{0}C before imaging. Time-lapse movies were acquired every 10 seconds for 10 minutes on a Leica M205 FA fluorescence stereomicroscope employing the GFP and mCherry filter sets (0.5 second exposure for each). Ookinete speeds were calculated on Fiji software (NIH, http://fiji.sc/Fiji) using the MtrackJ plugin [41].

Scanning and transmission electron microscopy

For scanning and transmission electron microscopy *P. berghei* gametocytes 8 hours post-activation (hpa) and 24hpa in ookinete medium were processed as described in [42]. SEM samples were examined on a JEOL6400 SEM running at 10kV and tiff images captured using Olympus Scandium software. TEM samples were examined either on Tecnai T20 (FEI) running at 200kV or Leo 912AB TEM running 120kV and images captured using Gatan Digital Micrograph Software (Gatan, Japan).

Inhibition of gametocyte fertilisation

To prevent fertilization of female gametes, unactivated gametocytes were cultured in enriched PBS (PBS supplemented with 2mM HEPES, 2mM Glucose, 0.4mM NaHCO3, 0.01% BSA) containing 100 mM 2-Deoxy-D-glucose (Sigma) for 45 minutes [22] and filtered through Plasmodipur filters (EuroProxima), washed with ookinete medium and re-cultured in ookinete medium without 2-Deoxy-D-glucose (2DG) for 24h. Female gametocytes activate but fertilization is prevented due to a blockage in male gamete exflagellation [22].

Western Blotting

For analysis of PbRAB11A and ookinete development markers, *P. berghei* schizonts were enriched with 55% Nycodenz solution in PBS; gametocytes and ookinetes were enriched by 53% Nycodenz solution in PBS following density gradient centrifugation [21]. Mixed asexual blood stage parasites collected from an infected mouse by cardiac puncture were filtered through CF11 cellulose columns (Whatman-GE Healthcare Life Sciences) to exclude mice white blood cells and immediately lysed with ice-cold erythrocyte lysis buffer (1.5M NH4Cl, 0.1M KHCO3, 0.01 EDTA) for 15 minutes on ice. Equal amounts of parasite material from mixed asexual stage, schizonts, gametocytes and ookinetes were lysed in Net2+ buffer (140 mM NaCl, 50 mM Tris- pH 7.4, 4mM Dithiothreitol, 0.01% Nonidet P-40) supplemented with complete EDTA free Protease Inhibitor Cocktail Tablets (Roche) (1 tablet/10ml) and suspended in 2X Laemmli sample buffer containing 15% (v/v) β-mercaptoethanol and separated on 10 or 12 % SDS polyacrylamide gels (Flowgen Biosciences) and visualized using ECL and X-ray films as described by[42]. Blots were probed with primary antibodies (Table S4 & S5) and HRP coupled secondary antibodies either Polyclonal Goat anti-Rabbit or anti-mouse Ig/HRP (Dako) (1:10000). For infrared based visualization, appropriate secondary antibodies were used (IRDye® 680LT Goat anti-mouse IgG and IRDye® 800CW Goat

anti-rabbit IgG antibodies) and nitrocellulose blots were scanned on Odyssey® Sa Infrared Imaging System (LI-COR Biosciences). Blots were stripped twice for 5 minutes each with 0.2M NaOH solution and intermittent washing with distilled water and re-blocked in 5% milk in PBS-Tween before re-probing with further antibodies (Table S4 & S5). Microneme secretion assay was performed as described by [42], samples were concentrated on an Amicon-ultra centrifugal filter, 50 K cut-off (Millipore), suspended in Laemmli sample buffer and analysed as above.

Immunofluorescence assay

Air dried thin smears of *P. berghei* ookinete or schizont or sporozoites and oocysts, obtained from midgut of *P. berghei* infected *Anopheles stephensi* crushed in PBS, were fixed with 4% EM grade paraformaldehyde (Electron Microscopy Science) for 10 minutes. Permeabilisation, blocking and incubation with primary and appropriate secondary antibodies (Table S4 & S5) was performed as described by [42] with additional last washes with 70% ethanol and absolute ethanol 1 min each, air-dried and mounted in VectaShield (Vectorlabs) containing DAPI (4', 6-diamidino-2-phenylindole) in glycerol for nuclear staining. Parasites were examined either under Delta Vision Epifluorescence microscope (Applied Precision). 100x objective, images were captured with CoolSNAP HQ camera (Photometrics) and deconvoluted using SoftWoRx software (Applied Precision) or under Axioplane2 (Zeiss) 100x objective, images were taken through HAMAMATSU ORCA_ER camera (HAMAMATSU) and Velocity software 4.1.0 (PerkinElmer). Images were processed using Fiji (NIH) as well as SoftWoRx explorer 1.3. Super-resolution images were captured through Elyra PS.1 super-resolution microscope (Zeiss) under 60x objective with sCMOS PCO camera and images were visualized with ZEN Black software (Zeiss) and processed with ZEN LITE software (Zeiss).

Flow Cytometry analysis

WT-GFP, activated unfertilised WT-GFP female gametes (AUFG) and $_{p}$*clag::rab11a* gametes were collected 4hpa and 24hpa in ookinete media and purified using 53% Nycodenz density gradient centrifugation, washed with enriched PBS twice and vigorously vortexed three times 10 seconds each to break the zygote/ookinete clumps. Parasites were incubated with anti-P25 mAb (1:1000) diluted in enriched PBS for 30 minutes, washed and re-probed with secondary antibodies Goat anti-mouse Alexa Fluor 633 (1:1000) and erythroid cell marker anti-Ter119 PE/Cy5 antibody (eBioscience) (1:500) diluted in enriched PBS (see Table S5 for antibodies) supplemented with 5 µM Hoechst 33342 for 30 minutes, washed twice with enriched PBS and once with FACS buffer (2% (v/v) Fetal Bovine Serum (defined), 0.05% (w/v) sodium azide (NaN3) and 2 mM EDTA in PBS) vortexed. Parasites were re-suspended in 1ml FACS buffer and parasite aggregates were removed by filtering through nylon filtration fabric NITEX 40 µm pore size (Cadisch Precision Meshes). Samples were run on a FACS CyAn (Beckman Coulter) equipped with a 405 nm, 488

nm and 633 nm laser and 5,000 to 10,000 events were acquired. Post-acquisition analysis was performed using Kaluza software (Beckman Coulter). The gating strategy was implemented to identify female gametes, zygote and ookinetes (GFP, P25 and Hoechst positive, Ter119 PE/Cy5 negative) from negative controls of uninfected RBCs (Ter119 PE/Cy5 positive), infected RBCs with asexual stages of parasites (Ter119 PE/Cy5 and Hoechst positive) and unstained samples. The DNA content was analysed by comparing the Hoechst 33342 stain levels of these parasites. Differentiation between mutant male and female gametocytes were not possible due to lack of two-colour background of mutants as shown by [44].

Transcriptomics

Unactivated gametocytes were immediately filtered through Plasmodipur filters at 37^0C before enrichment step or used to set up ookinete cultures. All samples were enriched with Nycodenz density gradient centrifugation and mixed vigorously with 1 ml TRIzol (Ambion-Life Technologies) and stored at -80^0C or immediately used for RNA isolation using RNAeasy Universal Mini kit (Qiagen) with on-column DNAse digestion by RNase-free DNase set (Qiagen) according to manufacturer's instructions. RNA quality was assessed through reverse transcriptase PCR performed using SuperScript® III Reverse Transcriptase kit (Life Technology) before transcriptomic analysis (Glasgow Polyomics: www.polyomics.gla.ac.uk). RNA Sequencing (RNA-Seq) reads were prepared (see Table S6 and S7 for parameters of RNA-Seq) using Life Technologies stranded mRNA library kit and sequencing was carried out on Life Technologies Ion Proton platform.

Fastq files were quality controlled using FastQC (http://www.bioinformatics.babraham.ac.uk/projects/fastqc/, version 0.10.1) and trimmed for adapters and with a quality threshold >2=20 using cutadapt [[45], version 1.6 version, "-m 16 -b GGCCAAGGCG -q 20"]. Reads were then aligned to the *Plasmodium berghei* ANKA genome [[46] PlasmoDB version 11.1] using Tophat [[47]. version 2.0.12 , "--keep-fasta-order -b2-D 20 --b2-R 3 --b2-N 1 --b2-L 20 --b2-i S,1,0.50 -g 10 -I 5000 --library-type fr-firststrand"]. In order to have maximum sensitivity to low abundance or divergent transcripts reads that failed to align with Tophat2 were extracted using bed tools (http://bedtools.readthedocs.org/en/latest/, version 2.19.1, "bamtofastq") and aligned to the same reference using bowtie2 local alignments [[48], version 2.2.1 , "--local -D 20 -R 3 -N 1 -L 20 -i S,1,0.50 --mm"]. The Tophat accepted hits and bow tie2 aligned reads were then merged to form the alignment for that sample using Picard tools (http://broadinstitute.github.io/picard/, version 1.112). Gene-level expression analysis was carried out using the cufflinks2 package [[49] version 2.2.1] using annotated genes only (PlasmoDB VERSION 11.1 GFF file). Differential expression was carried out using cuffdiff (version 2.2.1). Subsequent analyses were carried out using the CummeRbund package (http://compbio.mit.edu/cummeRbund/, version 2.0).

Generic GO slim terms were obtained through PlasmoDB.org and only Biological Process terms were shown for simplicity.

Processed data and raw read files have been deposited at GEO with the Accession number xxxxx (to be supplied)

Supplementary Tables:

Parasite	bite back day	infection observed after bite back	number of experiments
WT-GFP	18th and 22nd or 24th	yes, on day 3	n=3
pclag::rab11a		no infection until day14	

Table S1 showing *pclag::rab11a* parasites are unable to transmit through mosquitos.

Parasite	bite back day	infection observed after bite back	number of experiments
WT-GFP	18th and 24th	yes, on day 3	n=2
pama-1::rab11a		no infection until day14	

Table S2 showing *pama1::rab11a* parasites are unable to transmit through mosquitos.

Number	Primer sequence	*Restriction Site/s*
GU0013	TGCTCTAGAATGAATTTTAAATACAGTTTTATT	
GU0014	TGCTCTAGATTACATTACTATCACGTAAATAAC	
GU0052	AGAACACCTGGGTATTCTGG	
GU1620	TGACAAGCTTTTGGTATAAACCTAACTTCTCCAGG	*HindIII*
GU1621	GGATCCGCGGCCCTTTCTTATAATTACCTAAGGGC	*SacII*
GU1622	GGCGGTACCCTATTCCATTCACGTAAATGTTAGCA	*KpnI*
GU1623	CGCTGATATCCTCGAGTTTTATATCGTTTTATTTTATTAATATTTTTAATTTACAAAT	*EcoRV/XhoI*
GU1766	CGGGATCAGCAAAAATTGATGAAAG	
GU1767	GTAGCGAATTCTACGCCTATAG	

Table S3 Primers used for PCR amplifications, generation of plasmids and diagnostic PCRs.

Protein	Peptide used to raise antibody	Raised In	Ab dilution for immunofluorescence assays	Ab dilution for western blotting
Anti-MyoA	MAVTNEELKTAHKIVRRVS	Rabbit	1000	1000
Anti-DOZI	MAGKNILARAKNGTGKTAA	Rabbit	250	2500
Anti-CITH	ESTVALQNVRSYGTEGRRQPD	Rabbit	250	2500
Anti-GAP45	HKYENDSDKLETGSQLTL	Rabbit	1000	5000
Anti-GAP50	HKLGLKKRKTLDKVNSL	Rabbit	1000	1000

Anti-IMC1b	HDNEMPNMEKLYDQLSFQKC	Rabbit	1000	-
Anti-actinI	GNVKAGVAGDDAPRS	Rabbit	1000	1000
Anti-Rab11A	CRGKK INVDNDNDEDEKKTK	Rabbit	1000	1000
Anti-Rab11B	CKVDLAEEDETKRKVTYE	Rabbit	1000	1000
Anti-P28	CVSKPQAPGTGSETP	Rabbit	-	1000
Anti-CTRP	CLNGGETPHNSNMEFENVENNDGIIEEENEDFEVIDANDPMW	Rabbit	5000	5000
Anti-chitinase	HTEKQYKSLSHVDALC	Rabbit	4000	4000

Table S4 Peptide raised primary antibodies from Proteintech used for immunofluorescence or western blotting.

Source	Protein	Raised In	Ab dilution for immune-fluorescence assays	Ab dilution for western blotting	Ab dilution for FACS analysis
Prof. Takafumi Tsuboi, Japan. Grown and purified by Serotec	FITC and Cy3 tagged anti-P25	Rabbit	2000	-	-
Roche	anti-GFP mAb	Rabbit	-	2000	-
Proteintech	anti-P25 mAb	Mouse	-	-	1000
eBioscience	Anti-mouse TER-119 PE-Cyanine5	Mouse	-	-	500
N. Philip et al 2012	anti-PPKL	Rabbit	1000	1000	-
Helen Banks	anti α-tubulin	Mouse	2000	5000	-
Prof. Judith Green, NIMR, London	anti-MTIP	Rabbit	1000	1000	-
Abcam	anti-cMyc	Rabbit	-	1000	-

Table S5 Primary antibodies obtained from external sources, their dilutions used for immunofluorescence, western blotting or FACS analysis.

Samples	Set1		Set2		Set3	
	Trimmed	**Raw**	**Trimmed**	**Raw**	**Trimmed**	**Raw**
WT-GFP gametocytes	9999709	10631567	10333258	10910347	9424540	10202613
$_p$*clag::rab11a* gametocyte	7380562	7724709	7658106	8236185	7493549	8107180
WT-GFP Ookinetes	8330977	8781630	6913529	7396991	8082056	8607430
$_p$*clag::rab11a* ookinetes	7386774	7956256	9882800	10630975	8867802	9418792

Table S6 RNASeq reads trimmed and raw for three sets of parasite samples

Set1	
WT-GFP gametocytes1.merge.bam	
Stats for BAM file(s):	
Total reads: 8609950	
Mapped reads: 8609950	-100%
Forward strand: 4133611	-48.01%
Reverse strand: 4476339	-51.99%
Failed QC: 0	0%
Duplicates: 0	0%
Paired-end reads: 0	0%

$_p$*clag::rab11a* gametocytes1.merge.bam	
Stats for BAM file(s):	
Total reads: 3264448	
Mapped reads: 3264448	-100%
Forward strand: 2315093	-70.92%
Reverse strand: 949355	-29.08%
Failed QC: 0	0%
Duplicates: 0	0%
Paired-end reads: 0	0%

WT-GFP ookinetes1.merge.bam	
Stats for BAM file(s):	
Total reads: 5290409	
Mapped reads: 5290409	-100%
Forward strand: 2897080	-54.76%
Reverse strand: 2393329	-45.24%
Failed QC: 0	0%
Duplicates: 0	0%

Paired-end reads: 0	0%

***$_p$clag::rab11a* ookinetes1.merge.bam**	
Stats for BAM file(s):	
Total reads: 6317982	
Mapped reads: 6317982	-100%
Forward strand: 3486291	-55.18%
Reverse strand: 2831691	-44.82%
Failed QC: 0	0%
Duplicates: 0	0%
Paired-end reads: 0	0%

Set2

WT-GFP gametocytes2.merge.bam	
Stats for BAM file(s):	
Total reads: 8943276	
Mapped reads: 8943276	-100%

***$_p$clag::rab11a* gametocytes2.merge.bam**	
Stats for BAM file(s):	
Total reads: 5569828	
Mapped reads: 5569828	-100%

Forward strand: 4095083	-45.79%
Reverse strand: 4848193	-54.21%
Failed QC: 0	0%
Duplicates: 0	0%
Paired-end reads: 0	0%

Forward strand: 2492556	-44.75%
Reverse strand: 3077272	-55.25%
Failed QC: 0	0%
Duplicates: 0	0%
Paired-end reads: 0	0%

WT-GFP ookinetes2.merge.bam	
Stats for BAM file(s):	
Total reads: 3555698	
Mapped reads: 3555698	-100%
Forward strand: 1958254	-55.07%
Reverse strand: 1597444	-44.93%
Failed QC: 0	0%
Duplicates: 0	0%
Paired-end reads: 0	0%

$_p$*clag::rab11a* ookinetes2.merge.bam	
Stats for BAM file(s):	
Total reads: 7054508	
Mapped reads: 7054508	-100%
Forward strand: 3728459	-52.85%
Reverse strand: 3326049	-47.15%
Failed QC: 0	0%
Duplicates: 0	0%
Paired-end reads: 0	0%

Set3

WT-GFP gametocyte3.merge.bam	
Stats for BAM file(s):	
Total reads: 7128574	
Mapped reads: 7128574	-100%
Forward strand: 3587661	-50.33%
Reverse strand: 3540913	-49.67%
Failed QC: 0	0%
Duplicates: 0	0%
Paired-end reads: 0	0%

$_p$*clag::rab11a* gametocytes*3*.merge.bam	
Stats for BAM file(s):	
Total reads: 6836368	
Mapped reads: 6836368	-100%
Forward strand: 3348360	-48.98%
Reverse strand: 3488008	-51.02%
Failed QC: 0	0%
Duplicates: 0	0%
Paired-end reads: 0	0%

WT-GFP ookinetes3.merge.bam	
Stats for BAM file(s):	
Total reads: 5834001	
Mapped reads: 5834001	-100%
Forward strand: 3390716	-58.12%
Reverse strand: 2443285	-41.88%
Failed QC: 0	0%
Duplicates: 0	0%
Paired-end reads: 0	0%

$_p$*clag::rab11a* ookinetes3.merge.bam
Stats for BAM file(s):

Total reads: 4044348	
Mapped reads: 4044348	-100%
Forward strand: 2591261	-64.07%
Reverse strand: 1453087	-35.93%
Failed QC: 0	0%
Duplicates: 0	0%
Paired-end reads: 0	0%

Tables S7 Number of reads aligned to the genome of P. berghei ANKA for comparison with the original read counts.

Acknowledgements

The support of the imaging facility at WCIP. HP was an Evimalar Ph.D. student and the generous input of Prof. Freddy Frischknecht is gratefully acknowledged. Michael Rennie prepared some of the ookinetes for EM imaging. Financial support was obtained from the Wellcome Trust (083811/Z/07/Z; 107046/Z/15/Z, WT104111AIA); and the FP7-funded Network of Excellence "Evimalar" of the European Commission (Ref. 242095).

Figure Legends.

Figure 1. Rab11A expression and localization during *P. berghei* life cycle stages.
A. PbRab11A transcription profile in FPKM at ring - R, trophozoite - T, schizont - S, gametocyte - G and ookinete - O stage [50]. Gametocyte expression data is shown as the measurements of Otto et al with the proportions of male (blue) to female (red) expression as reported by [51]. **B.** Expression of PbRab11A in: A, mixed asexual stages; S, schizonts; G, unactivated gametocytes and O, ookinete **C.** Expression of PbRab11A post-activation of gametocytes i.e. zygote to ookinete development using rabbit anti-PbRab11A antibody. Asterisks indicate the additional small PbRab11A band in schizont and ookinete. hpa= hours post-activation of gametocytes. **D.** Localization of Rab11A in WT-GFP parasites determined through anti-PbRab11A antibody during blood stage: schizont (separated merozoites), mosquito stages: 6h zygote, ookinete, day 10 oocyst and midgut sporozoites. Inset shows magnified image of segmented merozoite tip in respective panels. Scale bar 5 µm, Inset scale bar 2 µm.

Figure 2. Mutant *$_p$clag::rab11a* and *$_p$ama-1::rab11a* do not make ookinetes and down-regulate PbRab11A.
A. Microscopy images of immunofluorescence on fixed parasites using anti-RAB11A and anti-P25 antibodies as indicated and DAPI as a nuclear stain. **B.** Fertilized *$_p$clag::rab11a* and *$_p$ama-1::rab11a* spherical ookinetes i.e. 24h post-activation showing enlarged nucleus (Images taken on Axioplan). Scale bars 5 µm. **C.** Plot of *$_p$clag::rab11a* and *$_p$ama-1::rab11a* ookinete development (n=3, mean +/-SD, two tailed student t test, p-value 0.0001). **D.** Western blot for Rab11A in *$_p$clag::rab11a* and *$_p$ama-1::rab11a* parasites at various life cycle stages probed with anti-PbRab11A, anti-c-MYC antibody. GFP is a loading control. Asterisks show the presence of extra bands in schizont and ookinete stages when the blot is probed with anti-PbRab11A antibody. A: Asexual mixed blood stage; S: Schizonts; G: enriched Gametocytes; O: ookinetes. **E.** Western blots showing the expression of Rab11A in zygotes and ookinetes produced by *$_p$clag::rab11a* at 2, 4, 6, 8 and 24hpa as well as in **A**ctivated **U**n**F**ertilised **G**ametocytes (AUFG) 6 and 24hpa. **F-I.** Data from live parasites stained with αP25-Cy3, run on an Imagestream^x MkII imaging flow cytometer and analysed in IDEAS^{TM} software. All figures show analysis of >750 activated cells after gating for activated parasites based on area focus, GFP and P25-Cy3 intensity (See Supplemental Fig S2+) **F.** Imaging flow cytometry (IFC) density plots showing the aspect ratio of the masked GFP image (X axis) (AspectRatio_AdaptiveErode(M02, Ch02, 84)) against the circularity of the masked GFP image (Circularity_AdaptiveErode(M02, Ch02, 84)) Percentage values show proportion of parasites falling into each gate as described. **G.** Left panel: Dot plot of ookinete development (Circularity_AdaptiveErode(M02,Ch02,84)/AspectRatio(M02,Ch02,84) against P25 intensity (Intensity_MC_Ch03) for the WT-GFP (blue) *$_p$clag::rab11a* (red) and *$_p$ama1::rab11a* (green). Right panel: Bar graph representation of data in left panel split into 4 gates as indicated below. Mean +/-SD and P value 2-tailed T test compared to the control line for each promoter swap line. **H.** Left panel: Dot plot of the ookinete development against a measurement of the periphery of the ookinete using the perimeter measurement feature in IDEAS^{TM} software for WT-GFP (blue) *$_p$clag::rab11a* (red) and *$_p$ama1::rab11a* (green). Right panel: Graphical representation of the data in the left panel for four gates as indicated below. Bars show median and interquartile range. **I.** Representative images from gates i-iv for each line showing overlay of channel 2 (GFP) (green) and channel 3 antiP25-Cy3 (magenta)

Figure 3. *$_p$clag::rab11a* parasites are unable to transmit through mosquitoes.
A. Plot of oocyst load in dissected midguts of WT-GFP or *$_p$clag::rab11a* fed mosquitoes (n=3, two tailed student t test, p-value 0.0001). **B.** Images of dissected midguts and salivary glands from WT-GFP and *$_p$clag::rab11a* parasites fed mosquitoes. **C.** Speed of WT-mCherry and *$_p$clag::rab11a* spherical ookinetes. 16 ookinetes for each genotype were measured; bottom and top boxes denote first and third quartiles respectively, whiskers denote minimum and maximum. P<0.0001 **D.** Representative path of WT-mCherry and *$_p$clag::rab11a* ookinetes for 10 minutes .

Figure 4. Ultrastructural analysis of *$_p$clag::rab11a* 8h zygotes.

A. SEM images of 8h $_p$*clag::rab11a* zygotes showing the typical small yet specific membrane extension (see white arrow) as compared to retort outgrowth in 8h WT-GFP zygotes. **B.** TEM images of 8h $_p$*clag::rab11a* zygotes showing integrity of Apical Ring (APR) with aperture (AP), IMC and subpellicular microtubules (Mt) . **C.** SEM of left, 24h WT-GFP and right, $_p$*clag::rab11a* "ookinetes", the apical prominence is arrowed in the latter. **D.** TEM images of 2 magnifications of 24hpa $_p$*clag::rab11a* "ookinetes" demonstrating the fully developed nature of the apical prominence.

Figure 5. Western and immunofluorescence microscopy of ookinete development and structural markers.
A. Western blots for WT-GFP and $_p$*clag::rab11a* gametocytes at 2,4,6,8 and 24hpa, and for AUFG at 6 and 24hpa using anti-GAP45, anti-GAP50, anti-P28, anti-MyoA, anti-MTIP, anti-DOZI, anti-CITH, anti-PPKL, anti-αTubulin, anti-Chitinase and anti-actin I antibodies. Actin I and α-Tubulin act as loading controls. Asterisks show down-regulated or delayed expression proteins in respective bands. **B.** Fixed WT-GFP ookinetes and $_p$*clag::rab11a* spherical ookinetes were probed with primary antibodies: anti-GAP45, anti-Chitinase or anti-IMC1b antibodies mixed with FITC-tagged anti-P25 antibody. Images shown are single slices of Deltavision deconvoluted Z stack. Scale bar 5 µm. **C-F**. Image galleries from IFC analysis. Samples were run on an Imagestream^x MkII imaging flow cytometer were analysed using IDEAS^{tm} software. Images are representative of over 200 gametocytes analysed. **C**. Live 30 min post activation (PA) parasites stained with anti-P25-Cy3 and Tubulin tracker (Invitrogen). Cells were gated for area, focus, GFP and absence of P25-Cy3 expression to identify male gametocytes. **D**. Live parasites 90 min PA gated for area, aspect ratio and tubulin tracker (Invitrogen) stain to identify free male gametocytes. **E**. Female gametocytes 4 hpa identified by gating for area, focus, GFP and P25-Cy3 expression. Overlaid images are shown for channel2 (GFP) and channel3 (P25-Cy3) and channel2 (GFP) and channel 5 (Tubulin tracker) and single channel images for Tubulin tracker and brightfield. Scale bar (lower left) = 7 µm. >200 female parasites were analysed and there was no difference in the proportion of parasites activating (P25-Cy3 positive) or displaying a prominent tubulin focus. **F**. Live parasites at 25 hpa stained with tubulin tracker after partial permeabilisation of cells with LysoPC (lower) and non-permeabilised cells (upper). Scale bar (for all images) = 7 µm.

Figure 6. Ookinetes deficient in Rab11a expression also are relatively deficient in protein secretion.
Representative Western blot analysis of culture parasite pellet and supernatants protein content analysing parasite pellets (P) after collection by centrifugation and in the remaining culture supernatant (S). Chitinase and CTRP are expected to be released and shed into the culture supernatant respectively. DOZI is an abundant cytoplasmic protein that acts as a control for cell lysis.

Figure 7: Proposed model Rab11A mediated delivery of plasma membrane in *P. berghei*.
Rab11A mediated vesicles are involved in the delivery the plasma membrane and transmembrane proteins to the growing tip or to the neck region of retort / zygote. These are also possibly involved in secretion, development and maintenance of cell shape, protein trafficking coordinating with cytoskeletal components. Blue dots with '?' suggest possible numbers of spindle poles in a zygote WT-GFP 6hpa retort showing possible site for membrane expansion either at the apical tip 'a' or neck region. Expanded cartoons of the apical regions of mutant and wild type parasites at 6hpa highlight the vesicles that lack RAB11A.

Supplementary data.

Figure S1. Genomic introduction of *pbrab11a* promoter swap constructs.
A. *P. berghei* RNA-Seq data for *rab11a, clag* and *ama-1* shown in FPKM [50]. **B.** Schematic of the generation of $_p$*clag::rab11a* and $_p$*ama-1::rab11a* parasites (Not to Scale). Diagnostic PCRs for integration of **(C)** $_p$*clag::rab11a* and **(D)** $_p$*ama-1:: rab11a* constructs into WT-GFP gDNA, respectively, showing the 5' and 3' integration of respective constructs (PCR fragment as annotated in the schematic in **B**). W indicates a fragment present only in WT-GFP parasites. DNA '+' is an unrelated positive PCR control (P28) and '-' is a no DNA template negative PCR control.

Figure S2. Development of sexual stages of $_p$*clag::rab11a* and $_p$*ama-1::rab11a* parasites mirrors that of wild type parasites.
A. Images of Giemsa stained $_p$*clag::rab11a* and $_p$*ama-1::rab11a* gametocytes; M, male gametocytes; F, female gametocytes. **B.** Exflagellation count of male gametocytes of $_p$*clag::rab11a* (n=4, mean +/-SD, two tailed student t test, p-value 0.9891) and $_p$*ama-1::rab11a* (n=3, mean +/-SD, two tailed student t test, p-value 0.4337). **C.** Ratio of male to female gametocytes in $_p$*clag::rab11a* (n=6, mean +/-SD, two tailed student t test, p value 0.00046) and $_p$*ama-1::rab11a* (n=3, mean +/-SD, two tailed student test, p-value 0.0111) parasites compared to WT-GFP.

Figure S3. Expression of PbRAB11B is unaffected by downregulation of PbRAB11A in $_p$*clag::rab11a* mutant parasites.
A. Western blot analysis of PbRAB11B expression following activation of gametocytes comparing wild type parasites with $_p$*clag::rab11a* and Activated UnFertilised Gametocytes (AUFG) across the time course of zygote to ookinete transition sampling at times indicated in hours. **B.** Immunofluorescence imaging of RAB11B expression at 24hpa in the same parasite lines when mature ookinetes should be present.

Figure S4. Imaging flow cytometry gating strategy to quantitate ookinete conversion rate
Dot plots and histograms showing the sequential gating strategy pipeline used to identify ookinetes and quantitate conversion rate. Files were acquired separately then merged in IDEAS software. Step 1 – gate R1 defined objects within a broad size range that includes infected RBC, gametocytes and ookinetes. Step 2- R2 includes cells positive for GFP. Step 3 – R3 gates on cells in focus on the Brightfield image. This gate is broad as we observe that some activated female gametocytes displayed a lower gradient RMS that is normal for focussed cells. Step 4 - Gate R4 allows us to select cells in focus in the GFP channel. Step 5 - Gate R5 selects for cells positive for P25-Cy3. The proportion of GFP positive cells that were also positive for P25-Cy3 was similar for the WT and the promoter swap lines. Step 6 - The next gate selects cells also in focus in the P25-CY3 channel. GFP positive cells include asexual stages and non activated gametocytes. Events positive for GFP and Cy3 not included for analysis include uninfected RBC that are autofluorescent as a result of the phenylhydrazine treatment given to enhance parasitaemia. Step 7 - To help exclude images containing debris or overlapping cells a mask was generated to allow selection of cells where the area of the brightfield image was sufficiently larger than that of the area of the GFP image (Area_adaptiveErode(M05,Ch05) And not Area (M02,Ch02)). (Other strategies to exclude debris included using a spot count feature to identify images containing a single object, or the threshold feature to analyse only the object within the image that was within the size and intensity criteria. In some cases images including doublets and debris were manually selected for exclusion from analysis). Step 8- To separate out the three merged files the object number vs time is plotted and three populations from the individual samples can be separated. Step 9 – Finally the circularity and aspect ratio features were generated on the adaptive erode (84%) mask for the GFP image and used to plot ookinete conversion. Similar strategies using the brightfield image and the Cy3 image were also successful and gave similar results. All gating strategies were justified by examining images of objects falling outwith the gates. Step 10 – In order to plot the ookinete development against other features the aspect ratio and circularity features were combined onto one axis. Statistics below show the number of cells included and the % of each population

falling into each gate. In this figure 507 refers to WT-GFP, G480 refers to $_p$*clag::rab11a* and G481 refers to $_p$*ama1::rab11a*.

Figure S5. IFC Images

Gallery of representative images from the ookinete gate IV (Figure 2G) for the WT parasite line (top) and the promoter swap mutant lines. Scale bar (lower left) 7 µm.

Figure S6 $_p$*clag::rab11a* spherical ookinetes undergo meiosis.

A. Flow cytometry analysis on FACsCYAN to illustrate DNA content of $_p$*clag::rab11a* gametocytes 4hpa. Parasites stained with DNA stain Hoechst 33342 were gated for activation using anti-P25 antibody and DNA content in these compared to WT-GFP gametocytes 4hpa and WT-GFP activated unfertilized female gametes (AUFG) 4hpa. FACS plots showing results of one of three independent experiments. **B.** bar graph shows percentage of 4N (zygotes completed meiosis), 2N (fertilized female gametes, meiosis is incomplete or blocked) and 1N (gametocytes or asexual) parasites. Data from AUFG was used to verify the gating strategy (n=3, mean +/-SD, two tailed student t test, p-value 0.129292).

Figure S7 Active *rab11a* is contributed by both male and female gametes.

A. Cross-fertilization of $_p$*clag::rab11a* with male defective (*P48/45*$^-$) and female defective (*p47*$^-$) mutants (n=3, mean +/- SD, two tailed student t test, p value 0.0001) and **B.** Representative Giemsa images of ookinetes and zygotes obtained 24h after (cross) fertilisation. The decondensed nuclei of the $_p$*clag::rab11a* zygotes are arrowed. Scale bar = 5µm.

Figure S8. $_p$*ama-1::rab11a* parasites are unable to transmit through mosquitoes.

A. Plot of oocyst load in dissected midguts of WT-GFP and $_p$*ama-1::rab11a* fed mosquitoes (n=2, two tailed student t test, p-value 0.0001). **B.** Fluorescent and bright field images of WT-GFP and $_p$*ama-1::rab11a* infected midguts and salivary glands.

Figure S9. Immunofluorescence microscopy for ookinete development and structural markers.

Fixed WT-GFP ookinetes and $_p$*clag::rab11a* spherical ookinetes were probed with primary antibodies: anti-DOZI, anti-CITH, anti-PPKL, anti-CTRP, anti-MyoA and anti-MTIP antibodies mixed with either FITC-tagged anti-P25 or anti-α tubulin antibodies. Except PPKL, all images shown are single slice of Deltavision deconvoluted Z stack. For PPKL, single slice images of Z stacks obtained from ELYRA 3D SIM microscope is shown. Scale bar 5 µm.

Figure S10. Dynamic localization of GAP45.

Time course immunofluorescence of WT-GFP and $_p$*clag::rab11a* zygotes for GAP45 and P25 [4h timepoint images are taken through Axioplan and 6h timepoint images are single slices of deconvoluted Z stack taken from Deltavision microscope]. Scale Bar 5 µm.

Figure S11. Significantly deregulated genes in WT gametocytes vs $_p$*clag::rab11A* gametocytes .

Summary of the expression levels of genes that are more than 2 fold altered in a comparison of wild type and *rab11a* KD gametocytes as assessed by RNAseq analysis.

Figure S12 The altered transcription profile of rab11a KD gametocytes does not significantly overlap with that of either DOZI and CITH KO gametocytes.

Venn diagram representation of the extent of similarity between the transcriptomes of $_p$*clag::rab11a, cithko* and *doziko* gametocytes.

Figure S13 Significantly deregulated genes in WT ookinetes vs $_p$*clag::rab11A* 24hpa forms.

Summary of the expression levels of genes that are more than 2 fold altered in a comparison of wild type and *rab11a* KD ookinetes as assessed by RNAseq analysis.

Supplementary Video 1 $_p$*clag::rab11a* ookinetes are non-motile

Video from which Fig 3D is derived showing Matrigel-embedded motile wild type ookinetes (expressing RFP) and non-motile largely spherical $_{p}$*clag::rab11a* 24 hpi forms ("ookinetes" expressing GFP).

References:

[1] W. J. Nelson, "Adaptation of core mechanisms to generate cell polarity," *Nature,* vol. 422, no. 6933, pp. 766-74, Apr 2003, doi: 10.1038/nature01602.

[2] J. Chant, "Cell polarity in yeast," *Trends Genet,* vol. 10, no. 9, pp. 328-33, Sep 1994.

[3] S. K. Muthuswamy and B. Xue, "Cell polarity as a regulator of cancer cell behavior plasticity," *Annu Rev Cell Dev Biol,* vol. 28, pp. 599-625, 2012, doi: 10.1146/annurev-cellbio-092910-154244.

[4] W. J. Nelson and C. Yeaman, "Protein trafficking in the exocytic pathway of polarized epithelial cells," *Trends Cell Biol,* vol. 11, no. 12, pp. 483-6, Dec 2001.

[5] G. W. Reuther and C. J. Der, "The Ras branch of small GTPases: Ras family members don't fall far from the tree," *Curr Opin Cell Biol,* vol. 12, no. 2, pp. 157-65, Apr 2000.

[6] P. D'Adamo *et al.*, "RAB GTPases and RAB-interacting proteins and their role in the control of cognitive functions," *Neurosci Biobehav Rev,* Jan 2014, doi: 10.1016/j.neubiorev.2013.12.009.

[7] E. Quevillon, T. Spielmann, K. Brahimi, D. Chattopadhyay, E. Yeramian, and G. Langsley, "The *Plasmodium falciparum* family of Rab GTPases," *Gene,* vol. 306, pp. 13-25, Mar 13 2003.

[8] O. Ullrich, S. Reinsch, S. Urbe, M. Zerial, and R. G. Parton, "Rab11 regulates recycling through the pericentriolar recycling endosome," *J Cell Biol,* vol. 135, no. 4, pp. 913-24, Nov 1996.

[9] C. Agop-Nersesian *et al.*, "Rab11A-controlled assembly of the inner membrane complex is required for completion of apicomplexan cytokinesis," *PLoS Pathog,* vol. 5, no. 1, p. e1000270, Jan 2009, doi: 10.1371/journal.ppat.1000270.

[10] J. E. Burke *et al.*, "Structures of PI4KIIIβ complexes show simultaneous recruitment of Rab11 and its effectors," *Science,* vol. 344, no. 6187, pp. 1035-8, May 2014, doi: 10.1126/science.1253397.

[11] C. W. McNamara *et al.*, "Targeting Plasmodium PI(4)K to eliminate malaria," (in eng), *Nature,* vol. 504, no. 7479, pp. 248-53, Dec 2013, doi: 10.1038/nature12782.

[12] E. E. Kelly, C. P. Horgan, and M. W. McCaffrey, "Rab11 proteins in health and disease," *Biochem Soc Trans,* vol. 40, no. 6, pp. 1360-7, Dec 1 2012, doi: 10.1042/bst20120157.

[13] T. D. Otto *et al.*, "A comprehensive evaluation of rodent malaria parasite genomes and gene expression," *BMC Biol,* vol. 12, no. 1, p. 86, Oct 2014, doi: 10.1186/s12915-014-0086-0.

[14] P. J. Bradley *et al.*, "Proteomic analysis of rhoptry organelles reveals many novel constituents for host-parasite interactions in *Toxoplasma gondii*," *J Biol Chem,* vol. 280, no. 40, pp. 34245-58, Oct 2005, doi: 10.1074/jbc.M504158200.

[15] A. Herm-Gotz *et al.*, "Rapid control of protein level in the apicomplexan *Toxoplasma gondii*," *Nature methods,* vol. 4, no. 12, pp. 1003-5, Dec 2007, doi: 10.1038/nmeth1134.

[16] G. R. Mair *et al.*, "Regulation of sexual development of *Plasmodium* by translational repression,", *Science,* vol. 313, no. 5787, pp. 667-9, Aug 4 2006, doi: 10.1126/science.1125129.

[17] A. Guerreiro *et al.*, "Genome-wide RIP-Chip analysis of translational repressor-bound mRNAs in the *Plasmodium* gametocyte," *Genome Biol,* vol. 15, no. 11, p. 493, 2014, doi: 10.1186/s13059-014-0493-0.

[18] B. Franke-Fayard *et al.*, "A *Plasmodium berghei* reference line that constitutively expresses GFP at a high level throughout the complete life cycle," *Mol Biochem Parasitol,* vol. 137, no. 1, pp. 23-33, Sep 2004, doi: 10.1016/j.molbiopara.2004.04.007.

[19] I. Siden-Kiamos *et al.*, "Stage-specific depletion of myosin A supports an essential role in motility of malarial ookinetes," *Cell Microbiol,* vol. 13, no. 12, pp. 1996-2006, Dec 2011, doi: 10.1111/j.1462-5822.2011.01686.x.

[20] E. C. Laurentino *et al.*, "Experimentally controlled downregulation of the histone chaperone FACT in *Plasmodium berghei* reveals that it is critical to male gamete fertility," *Cell Microbiol,* vol. 13, no. 12, pp. 1956-74, Dec 2011, doi: 10.1111/j.1462-5822.2011.01683.x.

[21] C. J. Janse *et al.*, "High efficiency transfection of *Plasmodium berghei* facilitates novel selection procedures," *Mol Biochem Parasitol,* vol. 145, no. 1, pp. 60-70, Jan 2006, doi: 10.1016/j.molbiopara.2005.09.007.

[22] A. Srivastava *et al.*, "Stage-Specific Changes in *Plasmodium* Metabolism Required for Differentiation and Adaptation to Different Host and Vector Environments," *PLoS Pathog,* vol. 12, no. 12, p. e1006094, Dec 2016, doi: 10.1371/journal.ppat.1006094.

[23] S. Bennink, M. J. Kiesow, and G. Pradel, "The development of malaria parasites in the mosquito midgut," *Cell Microbiol,* vol. 18, no. 7, pp. 905-18, Jul 2016, doi: 10.1111/cmi.12604.

[24] A. C. Engevik and J. R. Goldenring, "Trafficking Ion Transporters to the Apical Membrane of Polarized Intestinal Enterocytes," *Cold Spring Harb Perspect Biol,* vol. 10, no. 1, Jan 2 2018, doi: 10.1101/cshperspect.a027979.

[25] J. B. Pereira-Leal, A. N. Hume, and M. C. Seabra, "Prenylation of Rab GTPases: molecular mechanisms and involvement in genetic disease," *FEBS Lett,* vol. 498, no. 2-3, pp. 197-200, Jun 8 2001, doi: 10.1016/s0014-5793(01)02483-8.

[26] D. Chakrabarti *et al.*, "Protein farnesyltransferase and protein prenylation in *Plasmodium falciparum*," *J Biol Chem,* vol. 277, no. 44, pp. 42066-73, Nov 1 2002, doi: 10.1074/jbc.M202860200.

[27] S. Sebastian *et al.*, "A *Plasmodium* calcium-dependent protein kinase controls zygote development and transmission by translationally activating repressed mRNAs," *Cell Host Microbe,* vol. 12, no. 1, pp. 9-19, Jul 2012, doi: 10.1016/j.chom.2012.05.014.

[28] R. W. Moon *et al.*, "A cyclic GMP signalling module that regulates gliding motility in a malaria parasite," *PLoS Pathog,* vol. 5, no. 9, p. e1000599, Sep 2009, doi: 10.1371/journal.ppat.1000599.

[29] K. Kennedy, et al., "Delayed death in the malaria parasite *Plasmodium falciparum* is caused by disruption of prenylation-dependent intracellular trafficking. *PLoS Biol* vol. 17 No. 7: e3000376, Aug, 2019. https://doi.org/10.1371/journal.pbio.3000376

[30] B. Spreng *et al.*, "Microtubule number and length determine cellular shape and function in *Plasmodium*," *Embo j,* vol. 38, no. 15, p. e100984, Aug 1 2019, doi: 10.15252/embj.2018100984.

[31] P. C. C. Garnham, R. G. Bird, and J. R. Baker, "Electron microscope studies of motile stages of malaria parasites. IV. The fine structure of the sporozoites of four species of *Plasmodium*," *Transactions of The Royal Society of Tropical Medicine and Hygiene,* vol. 57, no. 1, pp. 27-31, 1963, doi: 10.1016/0035-9203(63)90007-5.

[32] N. S. Morrissette and L. D. Sibley, "Cytoskeleton of apicomplexan parasites," *Microbiol Mol Biol Rev,* vol. 66, no. 1, pp. 21-38; table of contents, Mar 2002, doi: 10.1128/mmbr.66.1.21-38.2002.

[33] R. E. Fowler, R. E. Fookes, F. Lavin, L. H. Bannister, and G. H. Mitchell, "Microtubules in *Plasmodium falciparum* merozoites and their importance for invasion of erythrocytes," *Parasitology,* vol. 117 (Pt 5), pp. 425-33, Nov 1998.

[34] B. Poulin *et al.*, "Unique apicomplexan IMC sub-compartment proteins are early markers for apical polarity in the malaria parasite," *Biol Open,* vol. 2, no. 11, pp. 1160-70, 2013, doi: 10.1242/bio.20136163.

[35] B. Mahajan *et al.*, "Centrins, cell cycle regulation proteins in human malaria parasite *Plasmodium falciparum*,", *J Biol Chem,* vol. 283, no. 46, pp. 31871-83, Nov 2008, doi: 10.1074/jbc.M800028200.

[36] J. Q. Tran, J. C. de Leon, C. Li, M. H. Huynh, W. Beatty, and N. S. Morrissette, "RNG1 is a late marker of the apical polar ring in *Toxoplasma gondii*," *Cytoskeleton (Hoboken),* vol. 67, no. 9, pp. 586-98, Sep 2010, doi: 10.1002/cm.20469.

[37] M. E. Francia and B. Striepen, "Cell division in apicomplexan parasites," *Nat Rev Microbiol,* Jan 2014, doi: 10.1038/nrmicro3184.

[38] R. Y. Orr, N. Philip, and A. P. Waters, "Improved negative selection protocol for *Plasmodium berghei* in the rodent malarial model," *Malar J,* vol. 11, p. 103, Mar 31 2012, doi: 10.1186/1475-2875-11-103.

[39] M. R. van Dijk *et al.*, "Three members of the 6-cys protein family of *Plasmodium* play a role in gamete fertility," *PLoS Pathog,* vol. 6, no. 4, p. e1000853, Apr 8 2010, doi: 10.1371/journal.ppat.1000853.

[40] M. R. van Dijk *et al.*, "A central role for P48/45 in malaria parasite male gamete fertility," *Cell,* vol. 104, no. 1, pp. 153-64, Jan 12 2001, doi: 10.1016/s0092-8674(01)00199-4.

[41] E. Meijering, O. Dzyubachyk, and I. Smal, "Methods for cell and particle tracking," *Methods Enzymol,* vol. 504, pp. 183-200, 2012, doi: 10.1016/B978-0-12-391857-4.00009-4.

[42] N. Philip, H. J. Vaikkinen, L. Tetley, and A. P. Waters, "A unique Kelch domain phosphatase in *Plasmodium* regulates ookinete morphology, motility and invasion," *PLoS One,* vol. 7, no. 9, p. e44617, 2012, doi: 10.1371/journal.pone.0044617.

[43] A. A. Religa, J. Ramesar, C. J. Janse, A. Scherf, and A. P. Waters, "*P. berghei* telomerase subunit TERT is essential for parasite survival," *PLoS One,* vol. 9, no. 9, p. e108930, 2014, doi: 10.1371/journal.pone.0108930.

[44] G. R. Mair *et al.*, "Universal features of post-transcriptional gene regulation are critical for *Plasmodium* zygote development," *PLoS Pathog,* vol. 6, no. 2, p. e1000767, Feb 2010, doi: 10.1371/journal.ppat.1000767.

[45] M. Martin, "Cutadapt removes adapter sequences from high-throughput sequencing reads," *EMBL.net Journal Bioinformatics in action,* vol. 17, 2011.

[46] C. Aurrecoechea *et al.*, "PlasmoDB: a functional genomic database for malaria parasites," *Nucleic Acids Res,* vol. 37, no. Database issue, pp. D539-43, Jan 2009, doi: 10.1093/nar/gkn814.

[47] D. Kim, G. Pertea, C. Trapnell, H. Pimentel, R. Kelley, and S. L. Salzberg, "TopHat2: accurate alignment of transcriptomes in the presence of insertions, deletions and gene fusions," *Genome Biol,* vol. 14, no. 4, p. R36, 2013, doi: 10.1186/gb-2013-14-4-r36.

[48] B. Langmead and S. L. Salzberg, "Fast gapped-read alignment with Bowtie 2," *Nat Methods,* vol. 9, no. 4, pp. 357-9, Apr 2012, doi: 10.1038/nmeth.1923.

[49] C. Trapnell, D. G. Hendrickson, M. Sauvageau, L. Goff, J. L. Rinn, and L. Pachter, "Differential analysis of gene regulation at transcript resolution with RNA-seq," *Nat Biotechnol,* vol. 31, no. 1, pp. 46-53, Jan 2013, doi: 10.1038/nbt.2450.

[50] T. D. Otto *et al.*, "A comprehensive evaluation of rodent malaria parasite genomes and gene expression," *BMC Biol,* vol. 12, p. 86, Oct 30 2014, doi: 10.1186/s12915-014-0086-0.

[51] L. M. Yeoh, C. D. Goodman, V. Mollard, G. I. McFadden, and S. A. Ralph, "Comparative transcriptomics of female and male gametocytes in *Plasmodium berghei* and the evolution of sex in alveolates," *BMC Genomics,* vol. 18, no. 1, p. 734, Sep 2017, doi: 10.1186/s12864-017-4100-0.

Figure 1

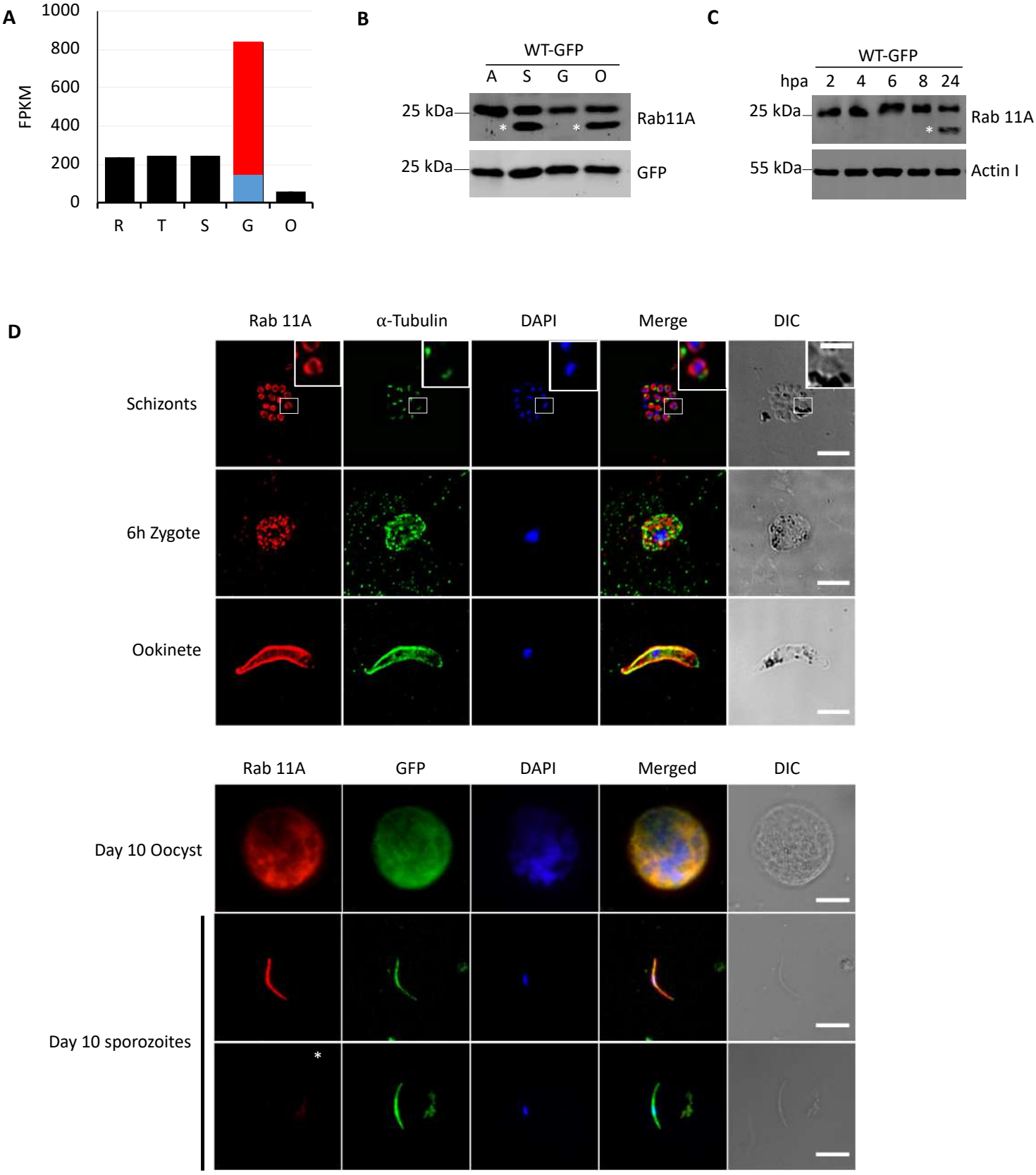
A
1000
800
600
400
200
0
FPKM
R
T
S
G
O
B
WT-GFP
A S G O
25 kDa
Rab11A
25 kDa
GFP
C
WT-GFP
hpa 2 4 6 8 24
25 kDa
Rab 11A
55 kDa
Actin I
D
Rab 11A
α-Tubulin
DAPI
Merge
DIC
Schizonts
6h Zygote
Ookinete
Rab 11A
GFP
DAPI
Merged
DIC
Day 10 Oocyst
Day 10 sporozoites

Figure 2

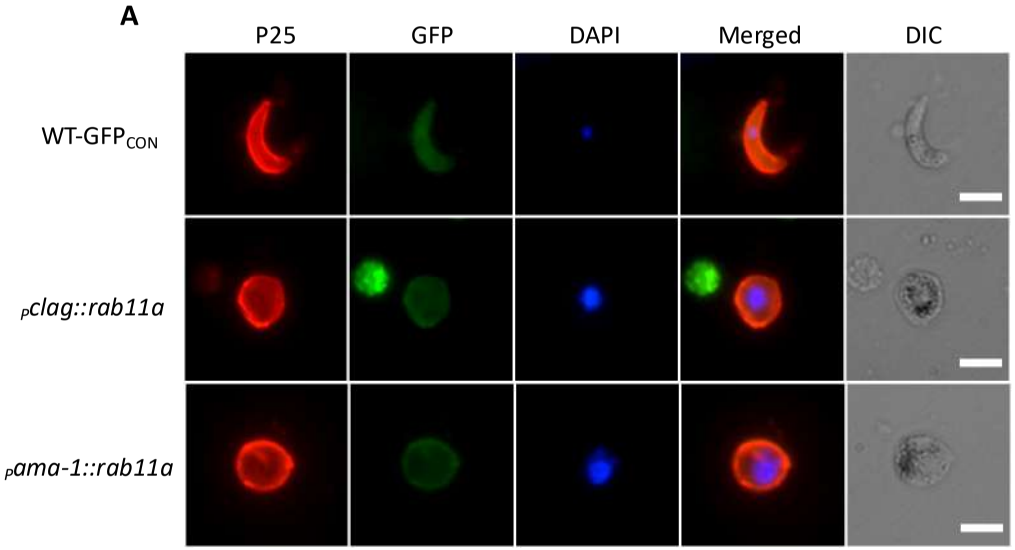
A
P25
GFP
DAPI
Merged
DIC
WT-GFP$_{CON}$
$_{P}$clag::rab11a
$_{P}$ama-1::rab11a

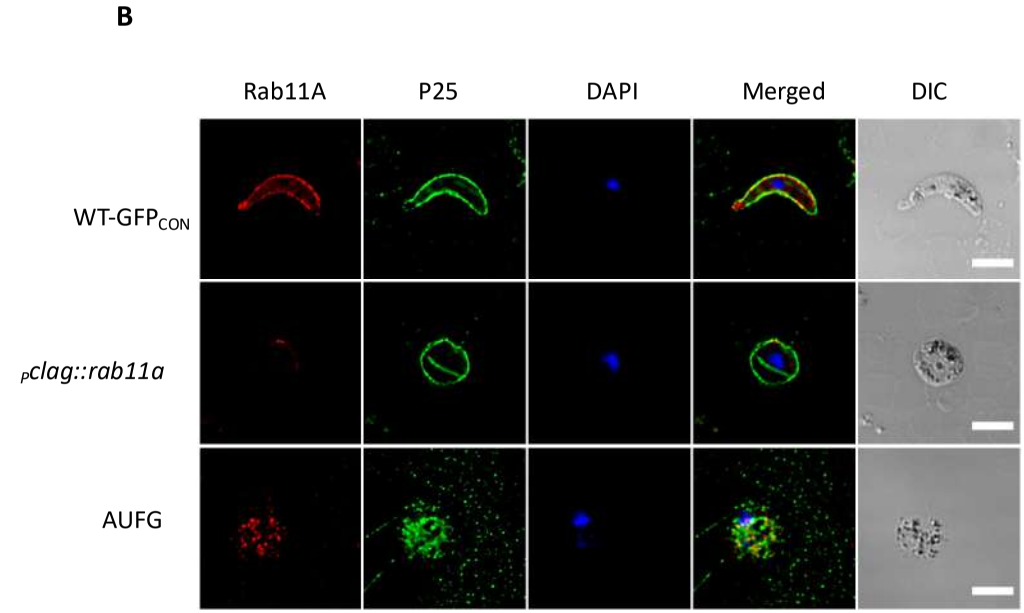
B
Rab11A
P25
DAPI
Merged
DIC
WT-GFP$_{CON}$
$_{P}$clag::rab11a
AUFG

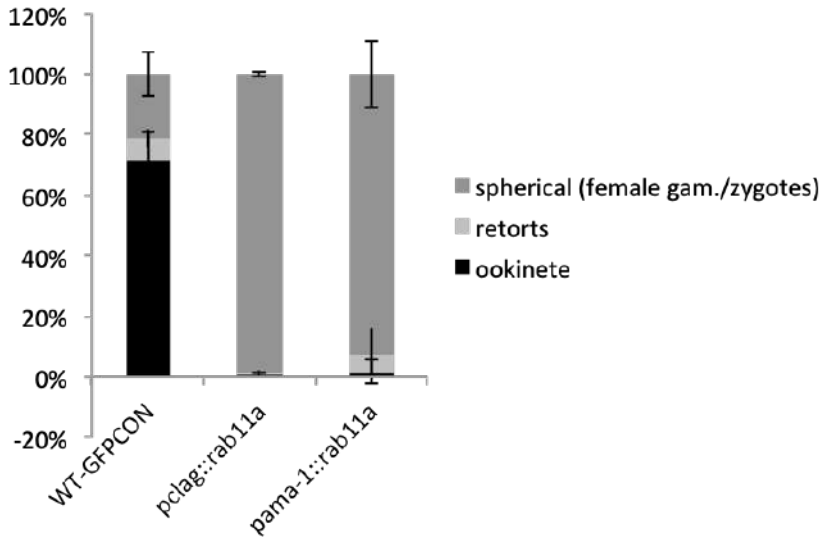
C
120%
100%
80%
60%
40%
20%
0%
-20%
WT-GFPCON
pclag::rab11a
pama-1::rab11a
spherical (female gam./zygotes)
retorts
ookinete

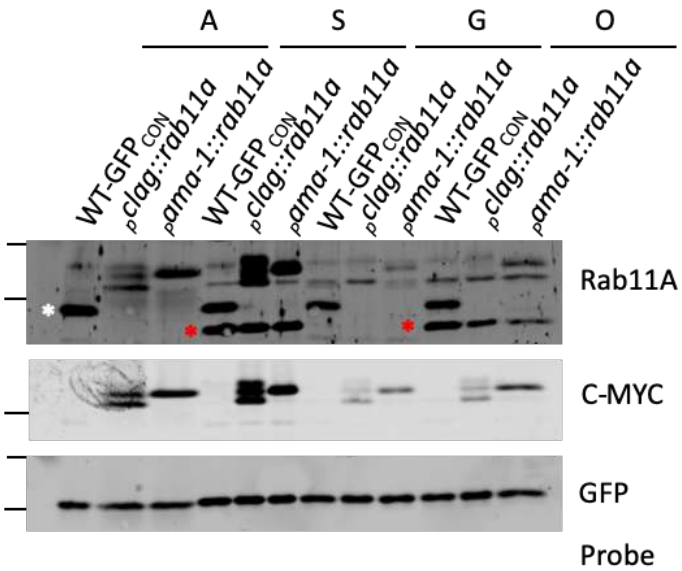
D
A
S
G
O
WT-GFP $_{CON}$
$_{P}$clag::rab11a
$_{P}$ama-1::rab11a
Rab11A
C-MYC
GFP
Probe

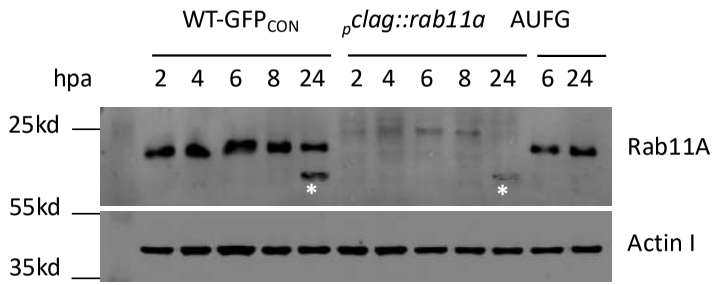
E
WT-GFP$_{CON}$
$_{P}$clag::rab11a
AUFG
hpa
2 4 6 8 24 2 4 6 8 24 6 24
25kd
55kd
35kd
Rab11A
Actin I

Figure 2

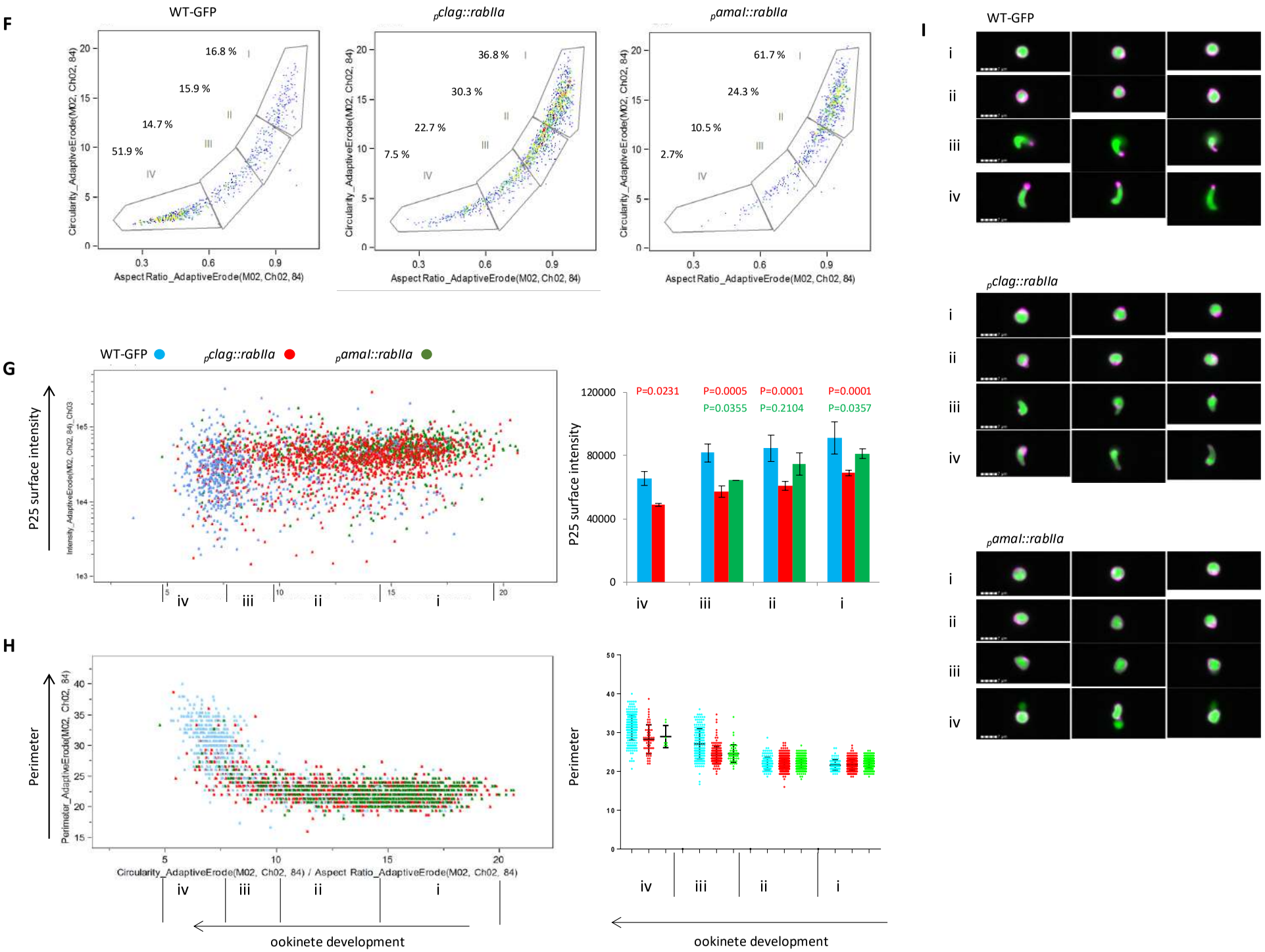
F
WT-GFP
pclag::rabIIa
pamal::rabIIa
16.8 %
15.9 %
14.7 %
51.9 %
36.8 %
30.3 %
22.7 %
7.5 %
61.7 %
24.3 %
10.5 %
2.7%
I
II
III
IV
Circularity_AdaptiveErode(M02, Ch02, 84)
Aspect Ratio_AdaptiveErode(M02, Ch02, 84)
G
WT-GFP
pclag::rabIIa
pamal::rabIIa
P25 surface intensity
P=0.0231
P=0.0005
P=0.0001
P=0.0001
P=0.0355
P=0.2104
P=0.0357
iv
iii
ii
i
H
Perimeter
Circularity_AdaptiveErode(M02, Ch02, 84) / Aspect Ratio_AdaptiveErode(M02, Ch02, 84)
ookinete development
I
WT-GFP
pclag::rabIIa
pamal::rabIIa

Figure 3

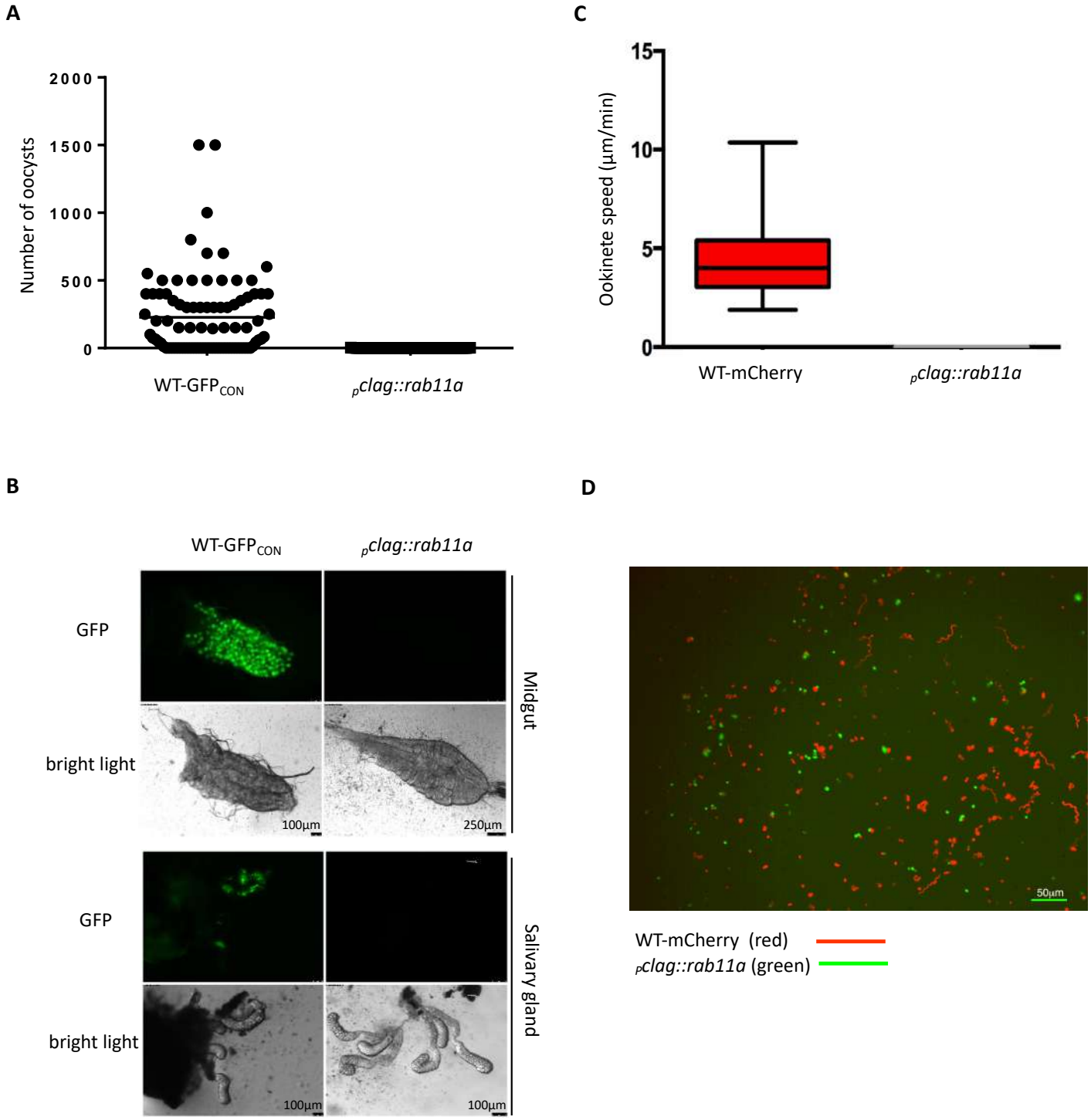
A
Number of oocysts
2000
1500
1000
500
0
WT-GFP$_{CON}$
$_p$clag::rab11a
C
Ookinete speed (µm/min)
15
10
5
0
WT-mCherry
$_p$clag::rab11a
B
WT-GFP$_{CON}$
$_p$clag::rab11a
GFP
bright light
100µm
250µm
Midgut
GFP
bright light
100µm
100µm
Salivary gland
D
50µm
WT-mCherry (red)
$_p$clag::rab11a (green)

Figure 4

A

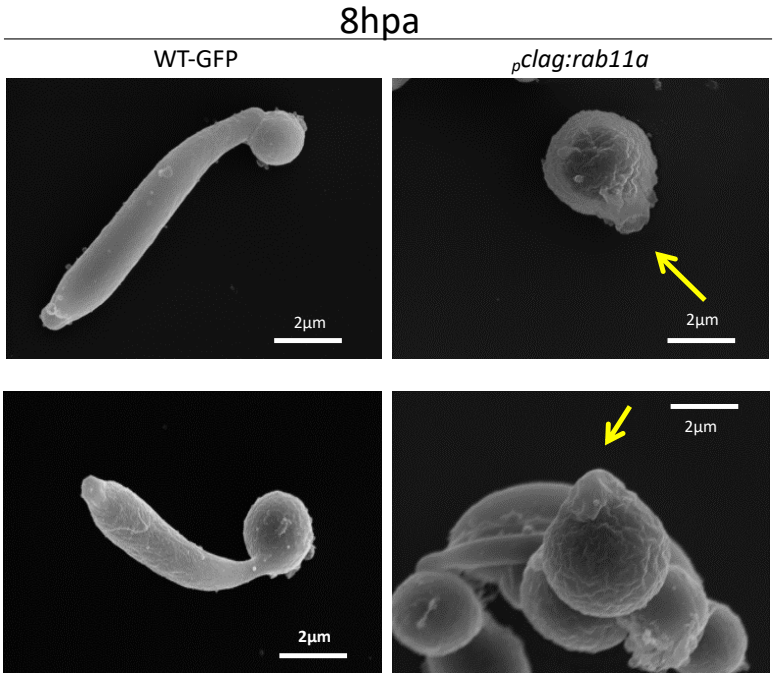
8hpa
WT-GFP
pclag:rab11a
2µm
2µm
2µm
2µm

B

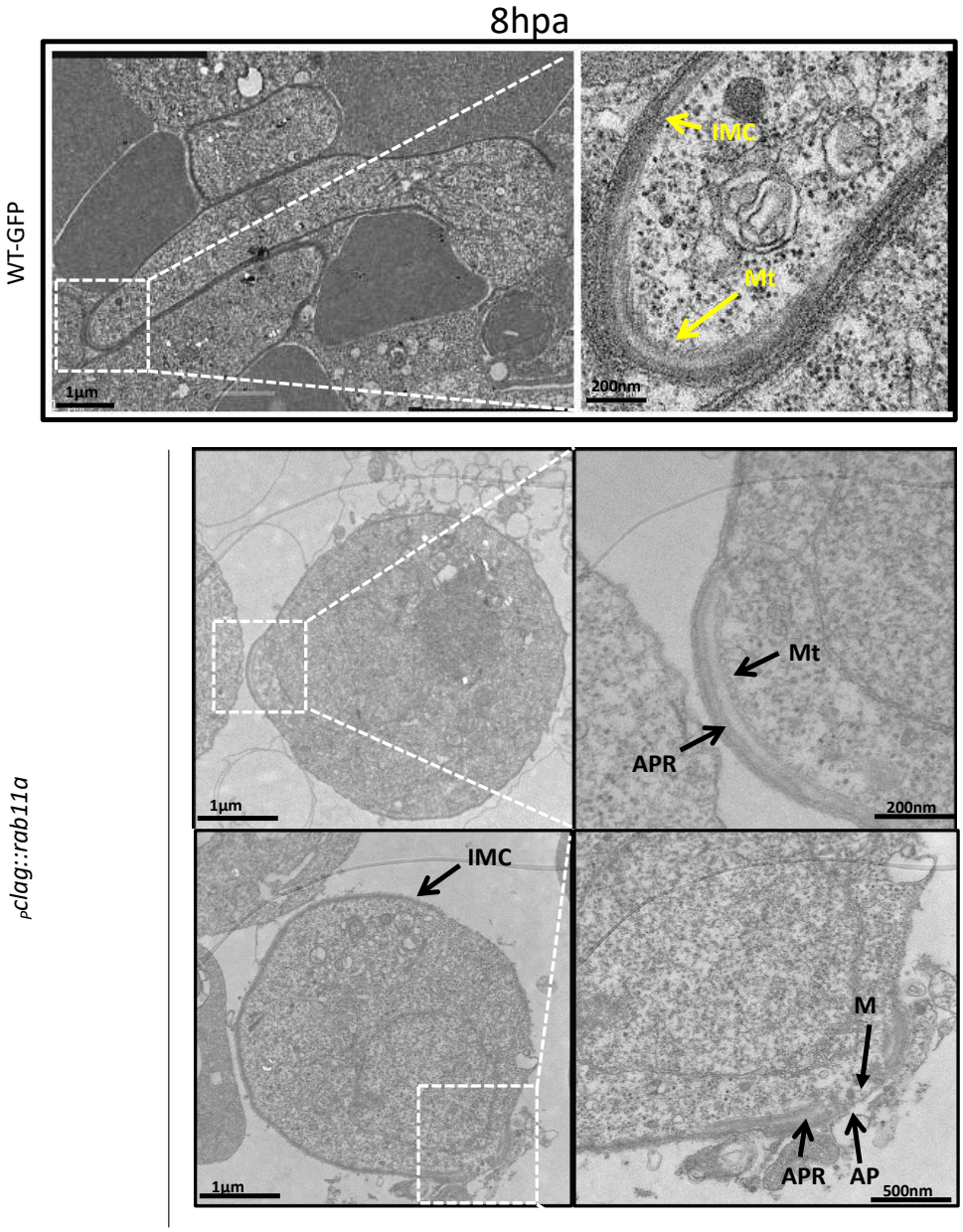
8hpa
WT-GFP
IMC
Mt
1µm
200nm
pclag::rab11a
Mt
APR
1µm
200nm
IMC
M
APR
AP
1µm
500nm

C

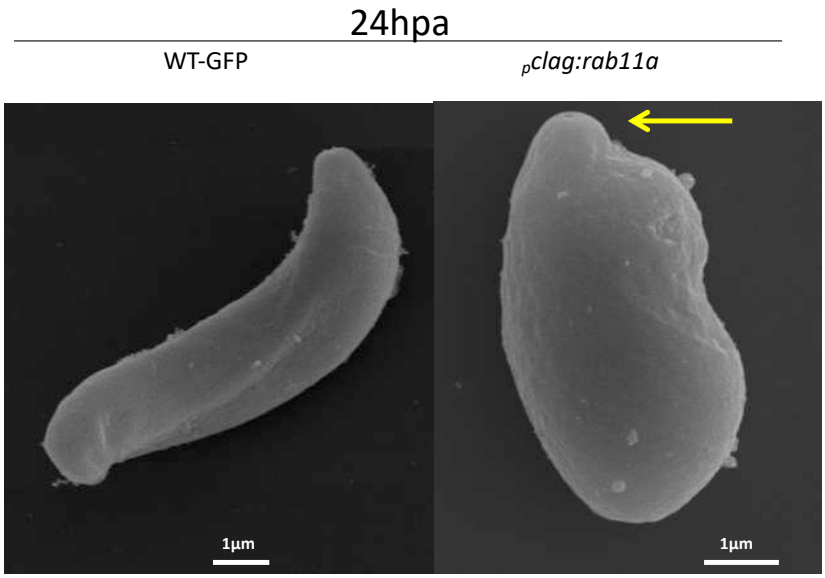

D

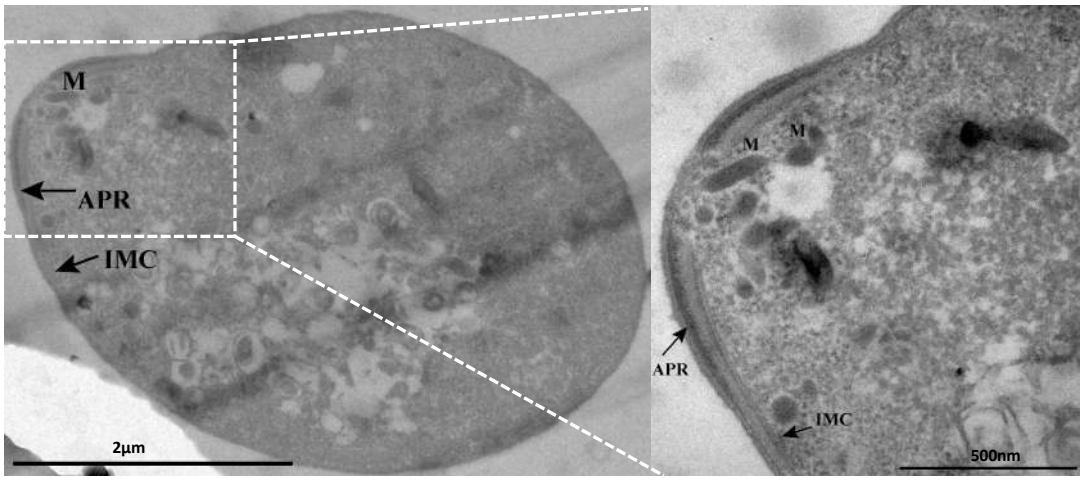

pclag:rab11a

Figure 5

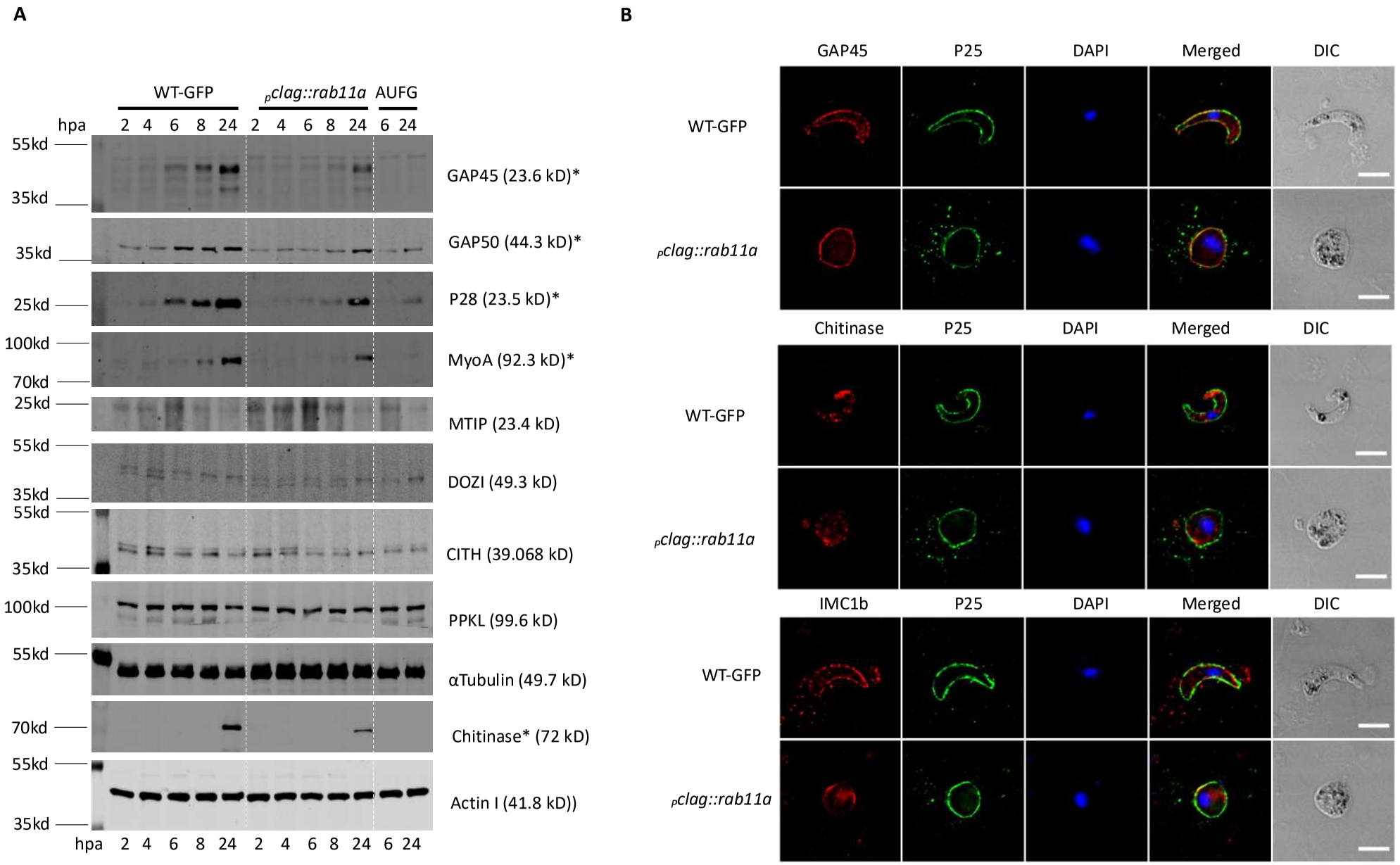
A
WT-GFP
pclag::rab11a
AUFG
hpa
2 4 6 8 24 2 4 6 8 24 6 24
55kd
35kd
GAP45 (23.6 kD)*
35kd
GAP50 (44.3 kD)*
25kd
P28 (23.5 kD)*
100kd
70kd
MyoA (92.3 kD)*
25kd
MTIP (23.4 kD)
55kd
35kd
DOZI (49.3 kD)
55kd
35kd
CITH (39.068 kD)
100kd
PPKL (99.6 kD)
55kd
αTubulin (49.7 kD)
70kd
Chitinase* (72 kD)
55kd
35kd
Actin I (41.8 kD))
B
GAP45
P25
DAPI
Merged
DIC
WT-GFP
pclag::rab11a
Chitinase
IMC1b

Figure 5

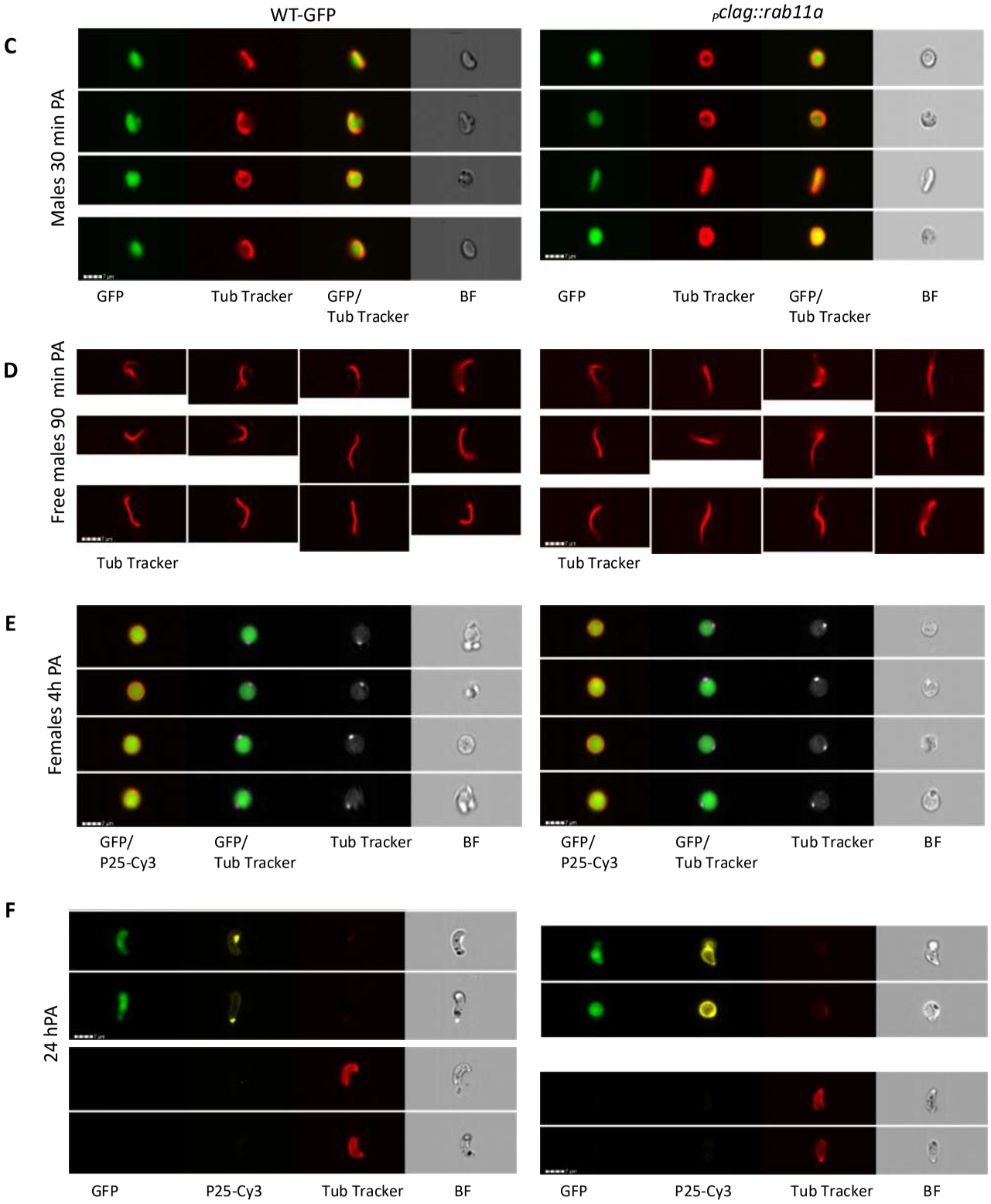
WT-GFP
pclag::rab11a
C
Males 30 min PA
GFP
Tub Tracker
GFP/
Tub Tracker
BF
GFP
Tub Tracker
GFP/
Tub Tracker
BF
D
Free males 90 min PA
Tub Tracker
Tub Tracker
E
Females 4h PA
GFP/
P25-Cy3
GFP/
Tub Tracker
Tub Tracker
BF
GFP/
P25-Cy3
GFP/
Tub Tracker
Tub Tracker
BF
F
24 hPA
GFP
P25-Cy3
Tub Tracker
BF
GFP
P25-Cy3
Tub Tracker
BF

Figure 6

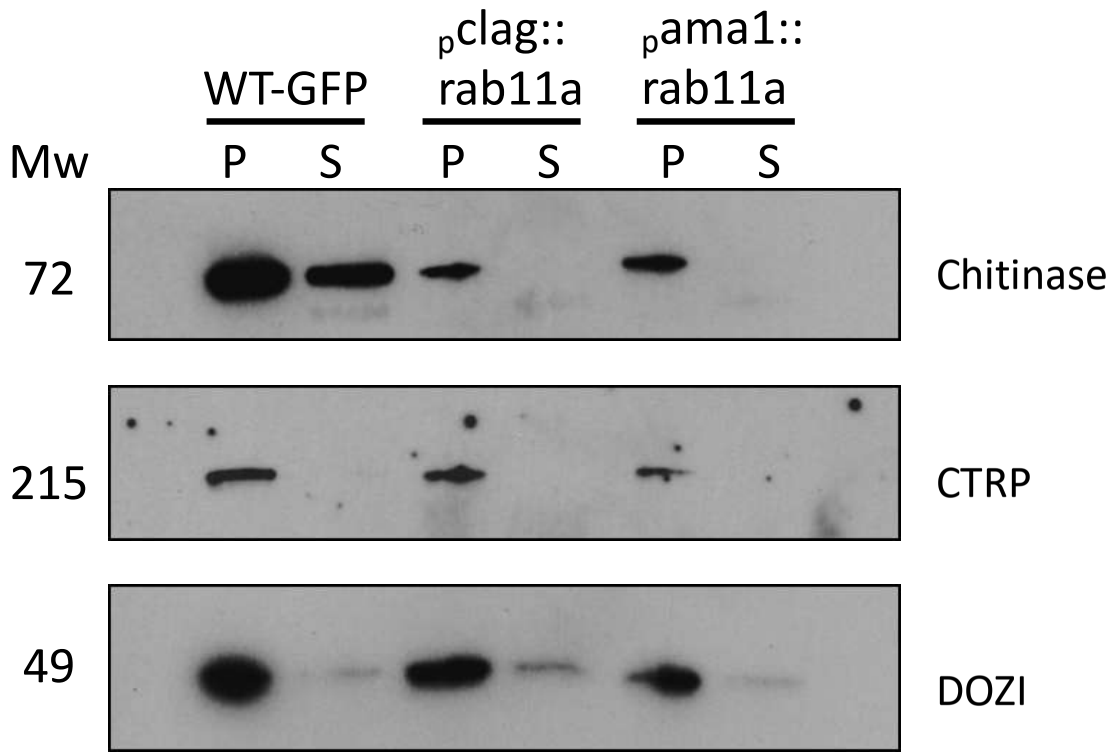
WT-GFP
pclag::
rab11a
pama1::
rab11a
Mw
P
S
P
S
P
S
72
Chitinase
215
CTRP
49
DOZI

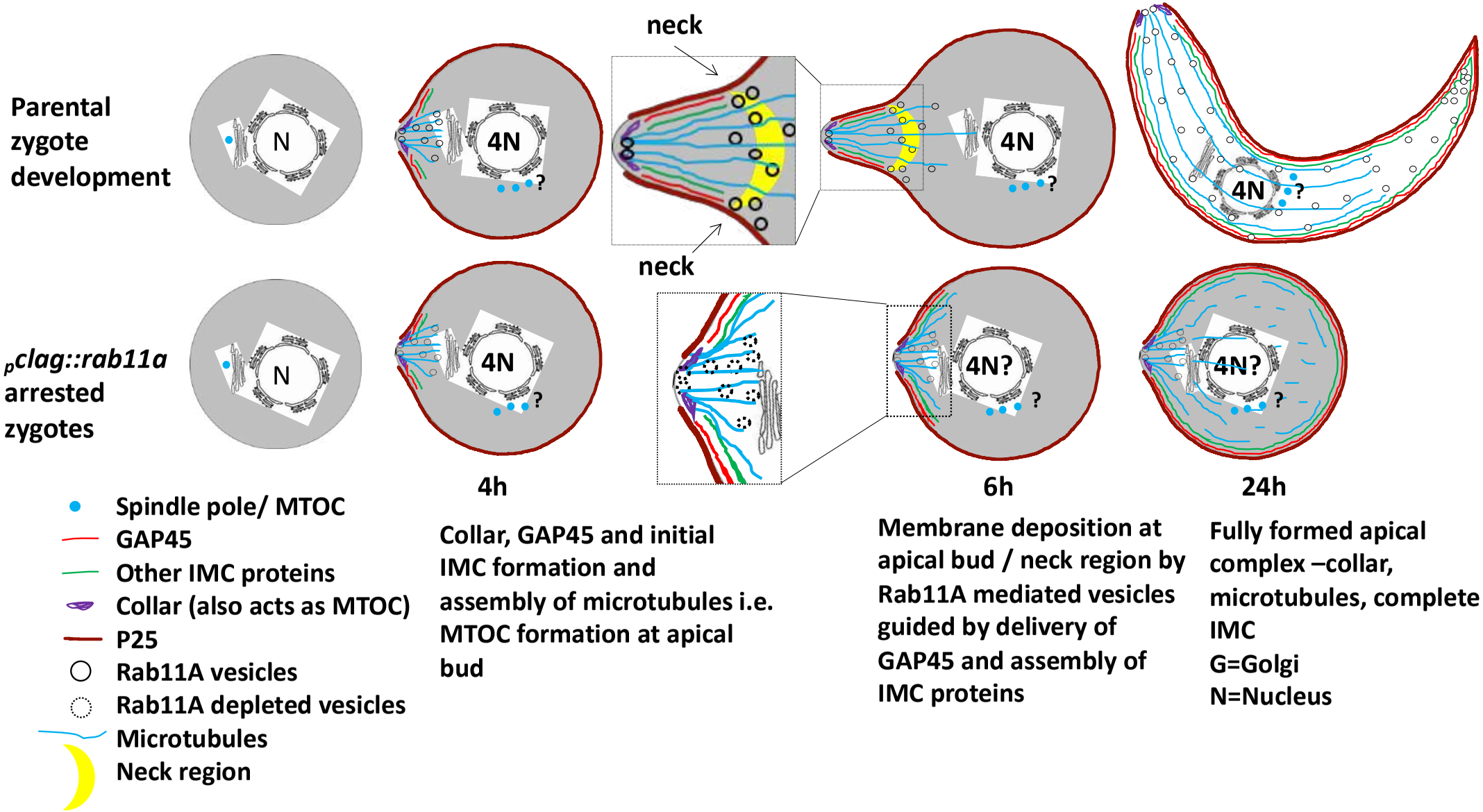
Parental zygote development
N
4N
?
neck
neck
4N
?
4N
?
$_p$clag::rab11a arrested zygotes
N
4N
?
4N?
?
4N?
?
4h
6h
24h
Spindle pole/ MTOC
GAP45
Other IMC proteins
Collar (also acts as MTOC)
P25
Rab11A vesicles
Rab11A depleted vesicles
Microtubules
Neck region
Collar, GAP45 and initial IMC formation and assembly of microtubules i.e. MTOC formation at apical bud
Membrane deposition at apical bud / neck region by Rab11A mediated vesicles guided by delivery of GAP45 and assembly of IMC proteins
Fully formed apical complex –collar, microtubules, complete IMC
G=Golgi
N=Nucleus

Figure S1

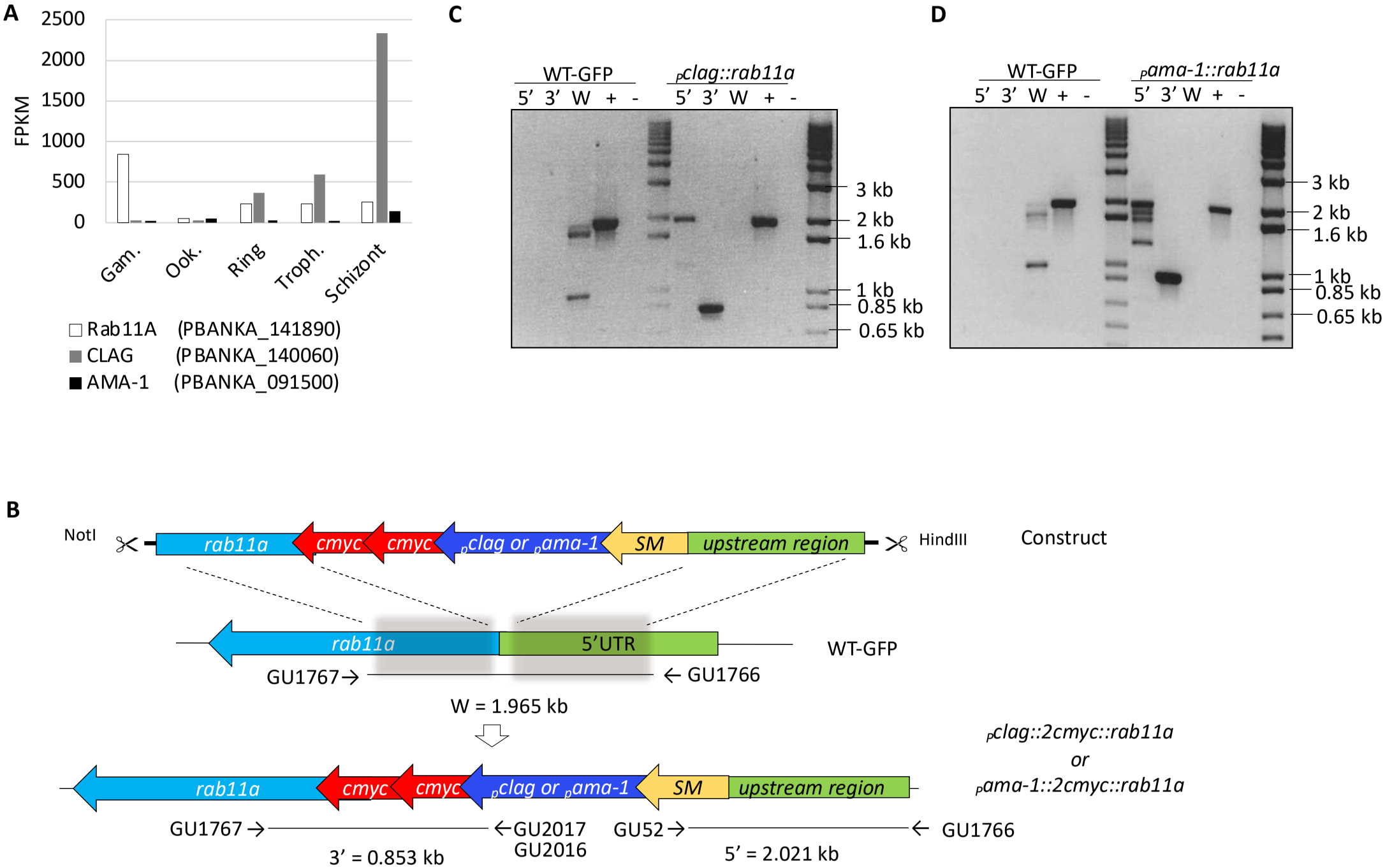
A
2500
2000
1500
1000
500
0
FPKM
Gam.
Ook.
Ring
Troph.
Schizont
Rab11A (PBANKA_141890)
CLAG (PBANKA_140060)
AMA-1 (PBANKA_091500)
C
WT-GFP
pclag::rab11a
5' 3' W + -
5' 3' W + -
3 kb
2 kb
1.6 kb
1 kb
0.85 kb
0.65 kb
D
WT-GFP
pama-1::rab11a
5' 3' W + -
5' 3' W + -
3 kb
2 kb
1.6 kb
1 kb
0.85 kb
0.65 kb
B
NotI
rab11a
cmyc
cmyc
pclag or pama-1
SM
upstream region
HindIII
Construct
rab11a
5'UTR
WT-GFP
GU1767
GU1766
W = 1.965 kb
pclag::2cmyc::rab11a
or
pama-1::2cmyc::rab11a
rab11a
cmyc
cmyc
pclag or pama-1
SM
upstream region
GU1767
GU2017
GU2016
GU52
GU1766
3' = 0.853 kb
5' = 2.021 kb

Figure S2

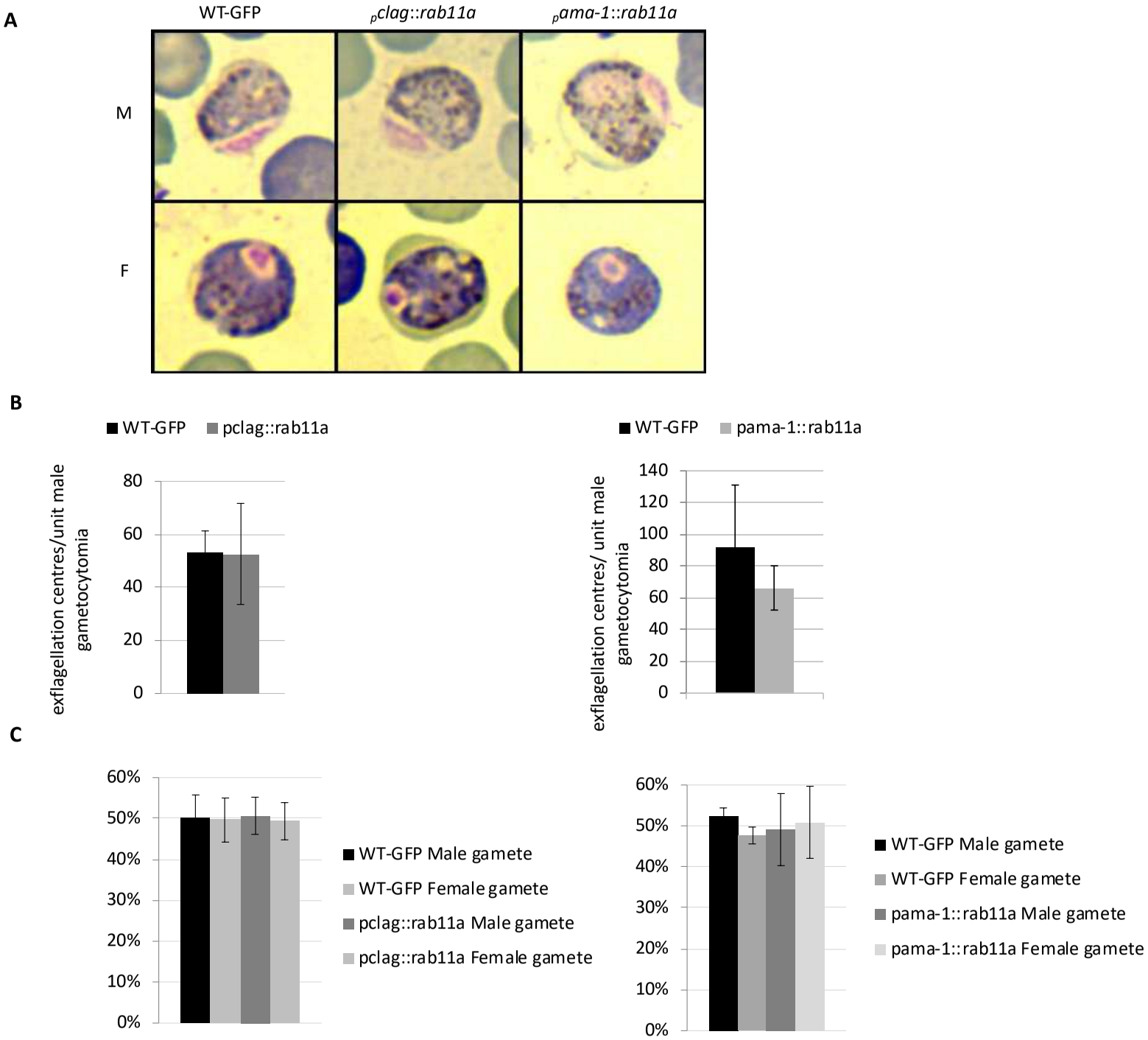
A
WT-GFP
pclag::rab11a
pama-1::rab11a
M
F
B
WT-GFP
pclag::rab11a
exflagellation centres/unit male gametocytomia
80
60
40
20
0
WT-GFP
pama-1::rab11a
exflagellation centres/ unit male gametocytomia
140
120
100
80
60
40
20
0
C
60%
50%
40%
30%
20%
10%
0%
WT-GFP Male gamete
WT-GFP Female gamete
pclag::rab11a Male gamete
pclag::rab11a Female gamete
WT-GFP Male gamete
WT-GFP Female gamete
pama-1::rab11a Male gamete
pama-1::rab11a Female gamete

Figure S3

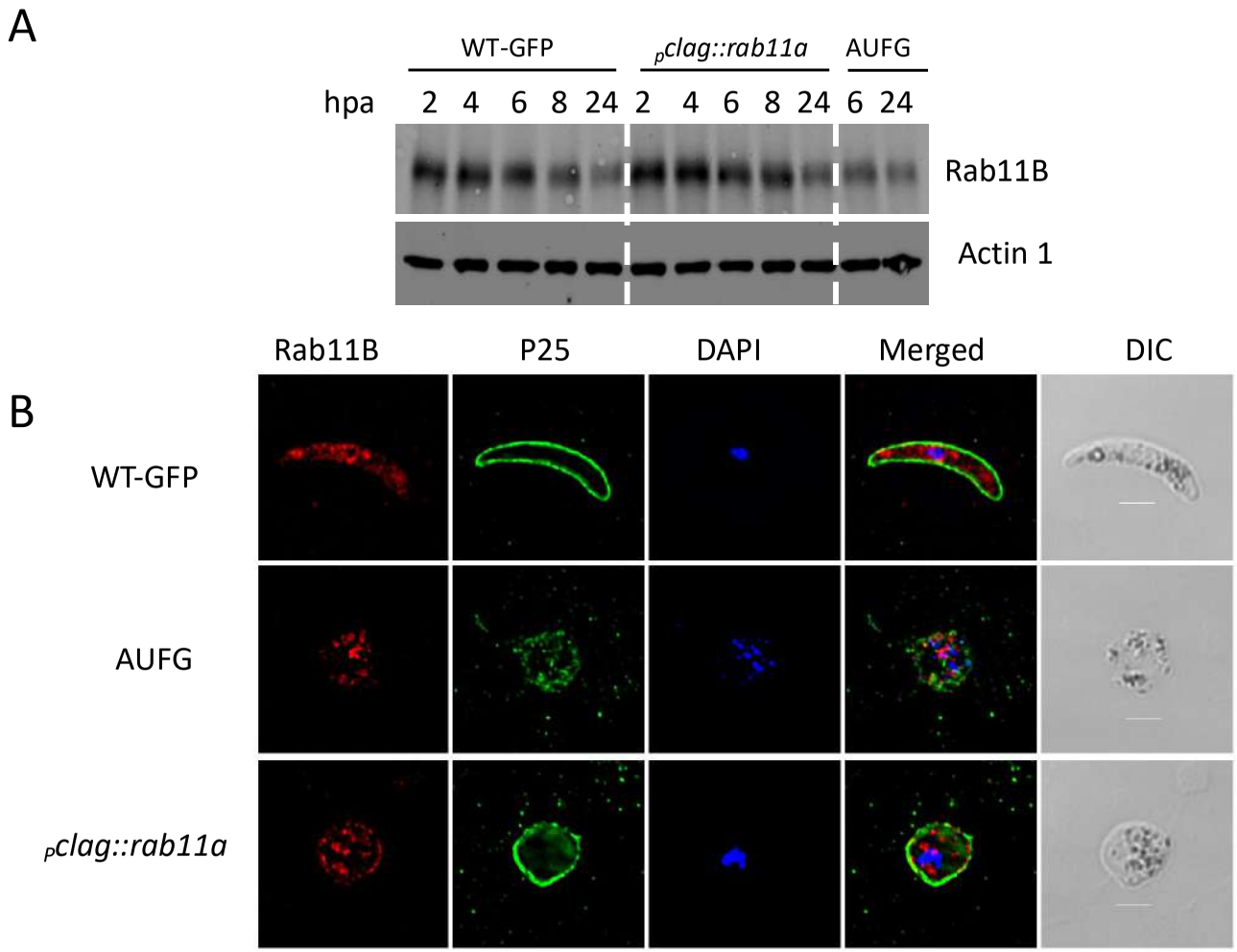
A
WT-GFP
pclag::rab11a
AUFG
hpa
2 4 6 8 24 2 4 6 8 24 6 24
Rab11B
Actin 1
B
Rab11B
P25
DAPI
Merged
DIC
WT-GFP
AUFG
pclag::rab11a

Figure S4

Imaging flow cytometry gating strategy to quantitate ookinete conversion rate

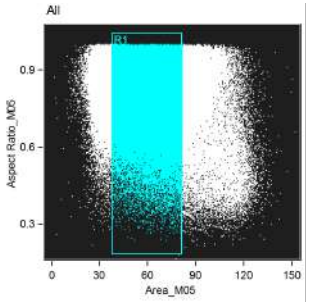

Area_M05, Aspect Ratio_M05

Population	Count	%Gated
All	519398	100
R1	389530	75

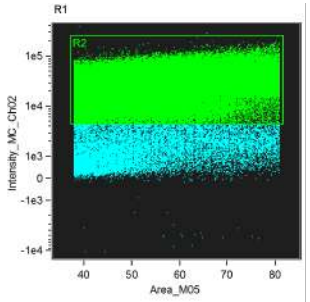

Area_M05, Intensity_MC_Ch02

Population	Count	%Gated
R1	389530	100
R2 & R1	371629	95.4

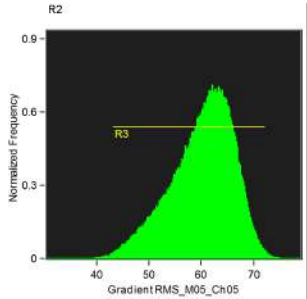

Gradient RMS_M05_Ch05

Population	Count	%Gated
R2 & R1	371629	100
R3 & R2 & R1	369272	99.4

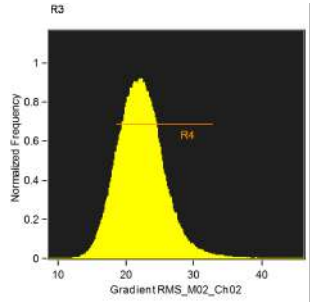

Gradient RMS_M02_Ch02

Population	Count	%Gated
R3 & R2 & R1	369272	100
R4 & R3 & R2 & R1	316533	85.7

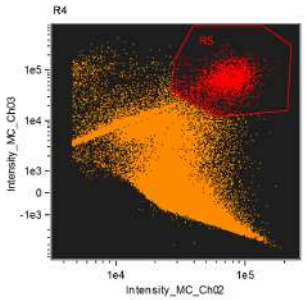

Intensity_MC_Ch02, Intensity_MC_Ch03

Population	Count	%Gated
R4 & R3 & R2 & R1	316533	100
R5 & R4 & R3 & R2 & R1	3361	1.06

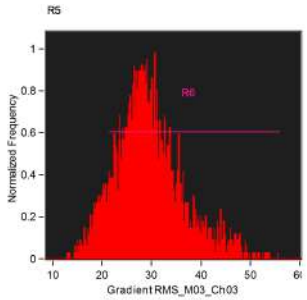

Gradient RMS_M03_Ch03

Population	Count	%Gated
R5 & R4 & R3 & R2 & R1	3361	100
R6 & R5 & R4 & R3 & R2 & R1	3008	89.5

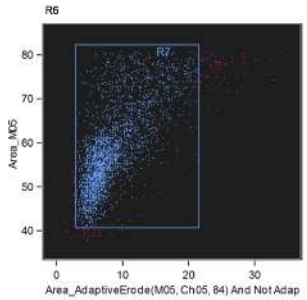

Area_AdaptiveErode(M05, Ch05, 84) And Not Adap, Area_M05

Population	Count	%Gated
R6 & R5 & R4 & R3 & R2 & R1	3008	100
R7 & R6 & R5 & R4 & R3 & R2...	2876	95.6

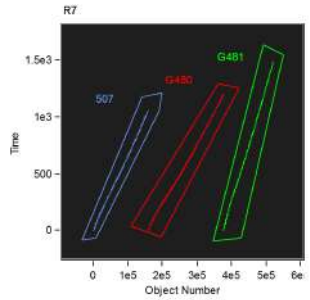

Object Number, Time

Population	Count	%Gated
R7 & R6 & R5 & R4 & R3 & R2...	2876	100
507 & R7 & R6 & R5 & R4 & R...	720	25
G480 & R7 & R6 & R5 & R4 & ...	1421	49.4
G481 & R7 & R6 & R5 & R4 & ...	735	25.6

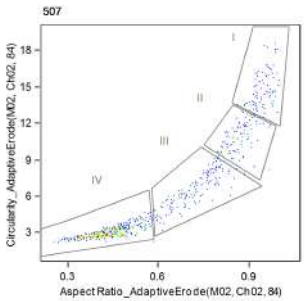

Aspect Ratio_AdaptiveErode(M02, Ch02, 84)

Population	Count	%Gated
507 & R7 & R6 & R5 & R4 & R...	720	100
I & 507 & R7 & R6 & R5 & R4...	88	12.2
II & 507 & R7 & R6 & R5 & R...	103	14.3
III & 507 & R7 & R6 & R5 & ...	148	20.6
IV & 507 & R7 & R6 & R5 & R...	371	51.5

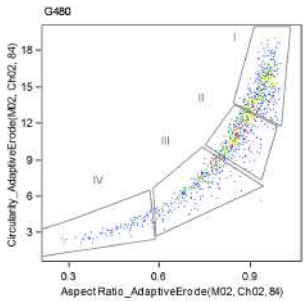

Aspect Ratio_AdaptiveErode(M02, Ch02, 84)

Population	Count	%Gated
G480 & R7 & R6 & R5 & R4 & ...	1421	100
I & G480 & R7 & R6 & R5 & R...	523	36.8
II & G480 & R7 & R6 & R5 & ...	430	30.3
III & G480 & R7 & R6 & R5 &...	323	22.7
IV & G480 & R7 & R6 & R5 & ...	106	7.46

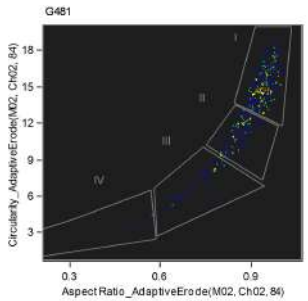

Aspect Ratio_AdaptiveErode(M02, Ch02, 84)

Population	Count	%Gated
G481 & R7 & R6 & R5 & R4 & ...	735	100
I & G481 & R7 & R6 & R5 & R...	421	57.3
II & G481 & R7 & R6 & R5 & ...	188	25.6
III & G481 & R7 & R6 & R5 &...	94	12.8
IV & G481 & R7 & R6 & R5 & ...	13	1.77

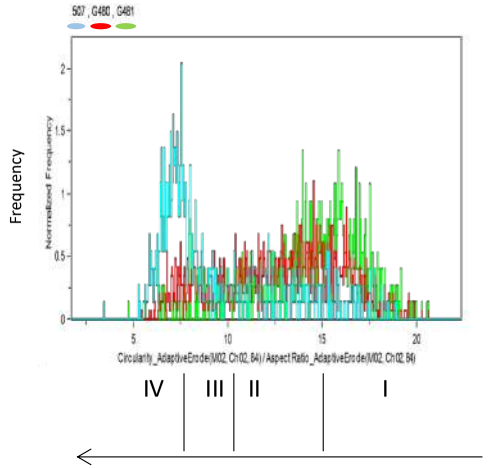

Figure S5

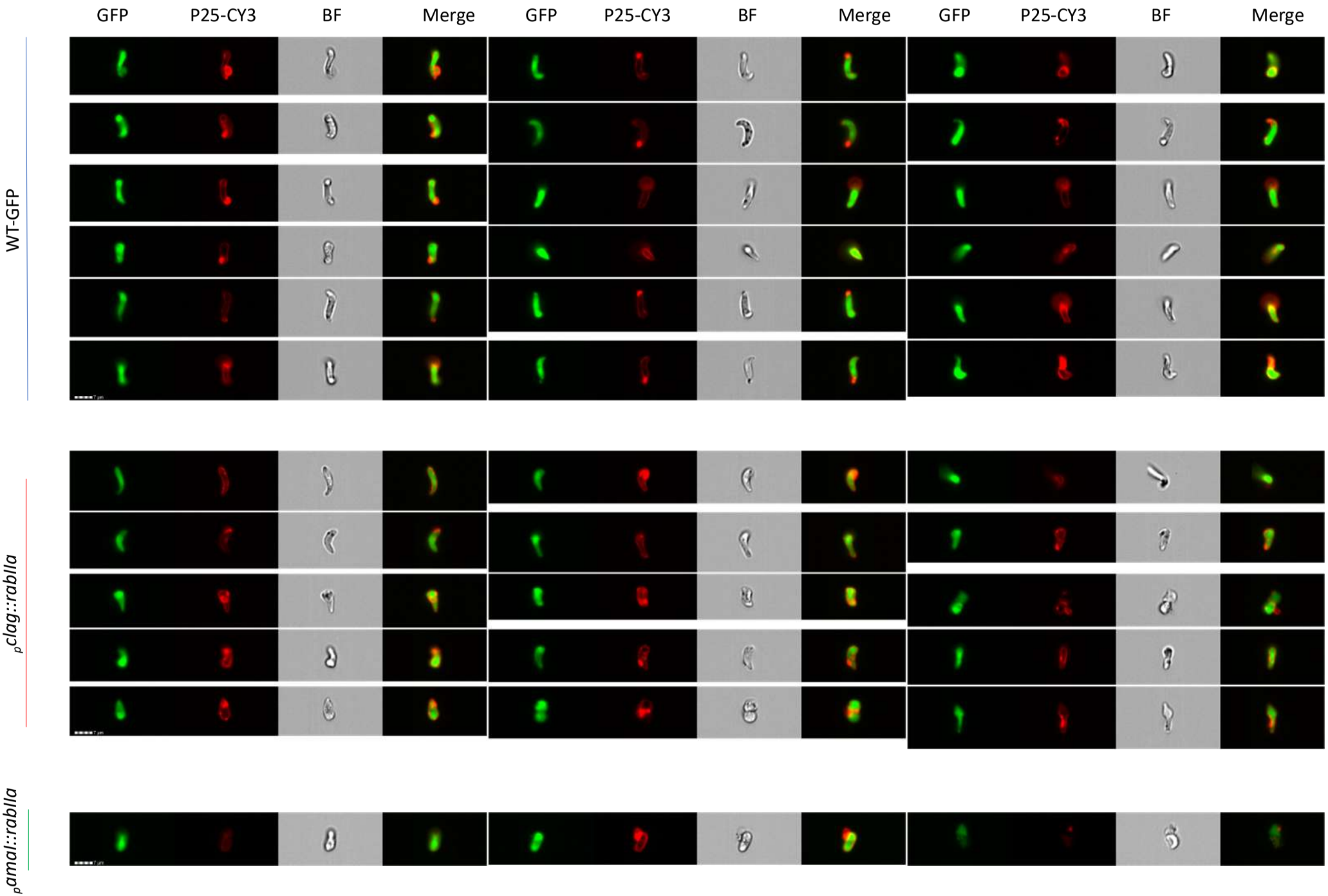
GFP
P25-CY3
BF
Merge
GFP
P25-CY3
BF
Merge
GFP
P25-CY3
BF
Merge
WT-GFP
pclag::rablla
pamal::rablla

Figure S6

A

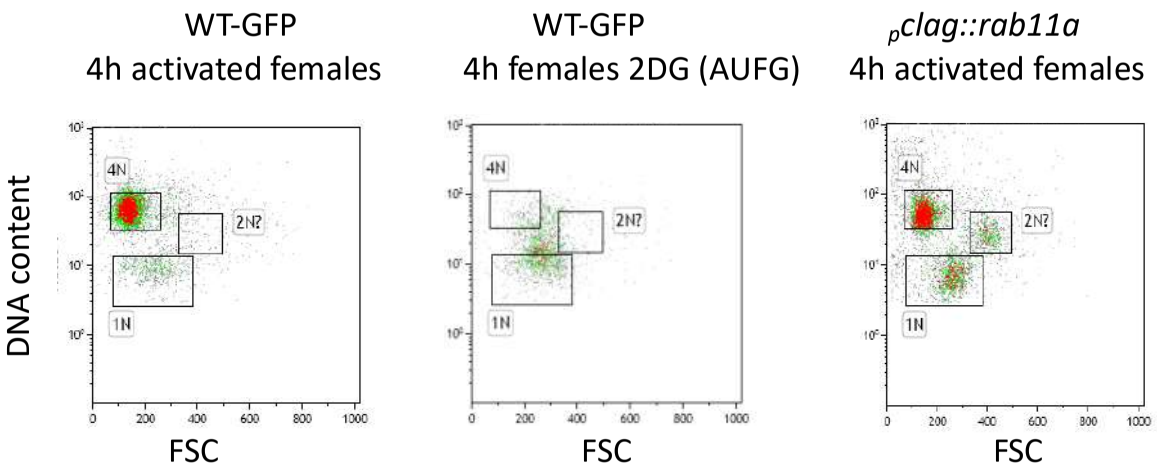
WT-GFP
4h activated females
WT-GFP
4h females 2DG (AUFG)
pclag::rab11a
4h activated females
DNA content
FSC
FSC
FSC
4N
2N?
1N
0
200
400
600
800
1000

B

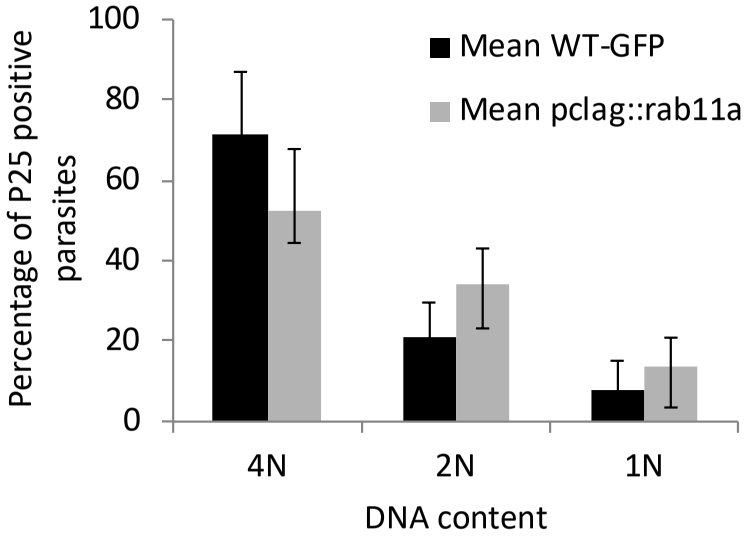
Percentage of P25 positive parasites
100
80
60
40
20
0
Mean WT-GFP
Mean pclag::rab11a
4N
2N
1N
DNA content

Figure S7

A

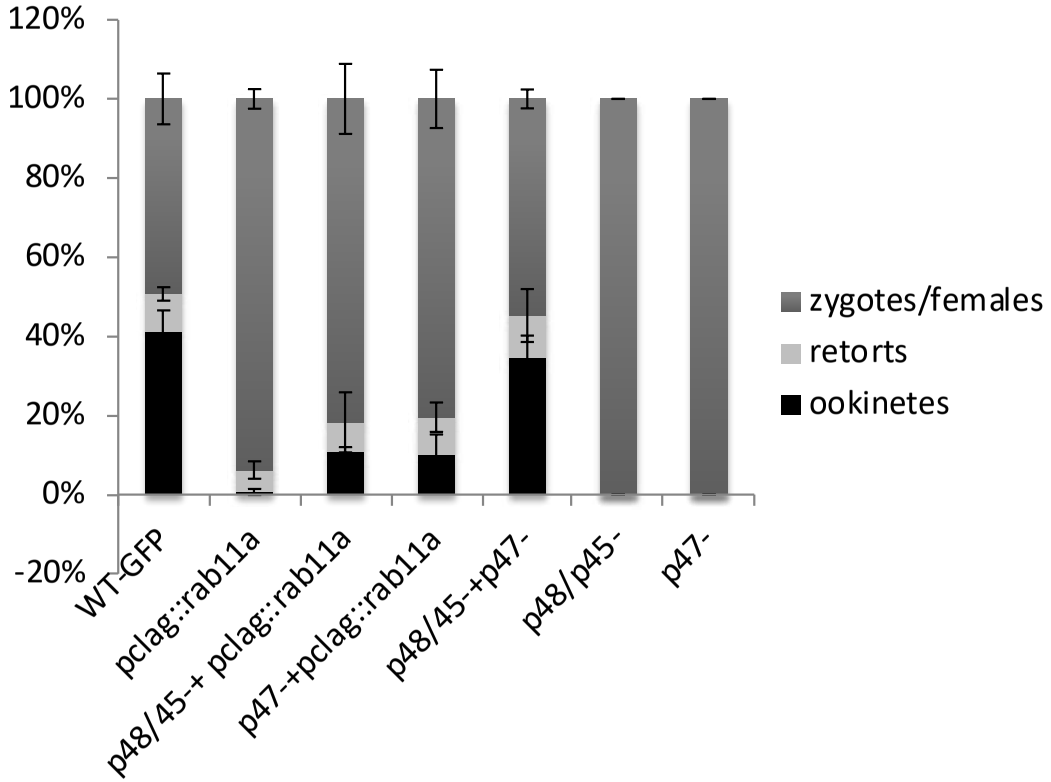
120%
100%
80%
60%
40%
20%
0%
-20%
WT-GFP
pclag::rab11a
p48/45-+ pclag::rab11a
p47-+pclag::rab11a
p48/45-+p47-
p48/p45-
p47-
zygotes/females
retorts
ookinetes

B

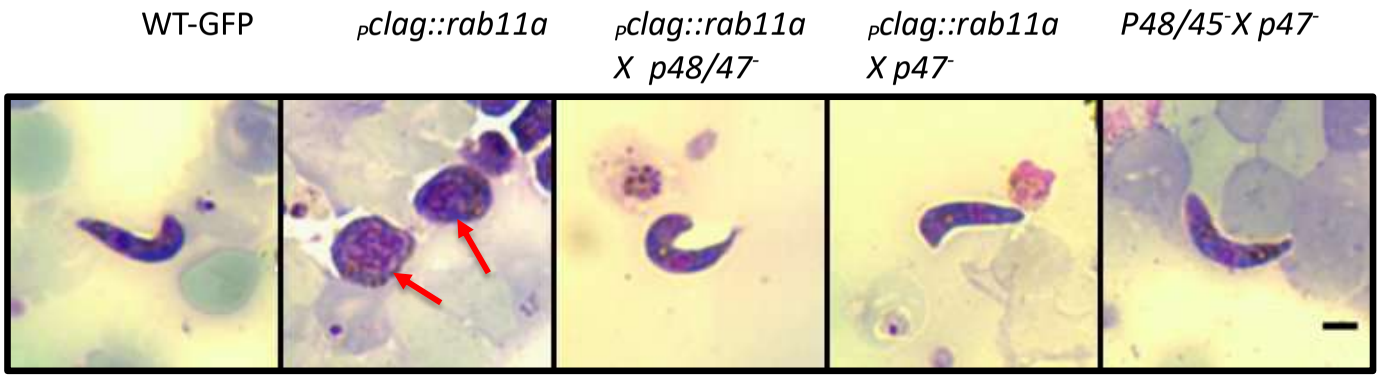
WT-GFP
pclag::rab11a
pclag::rab11a X p48/47-
pclag::rab11a X p47-
P48/45-X p47-

Figure S8

A

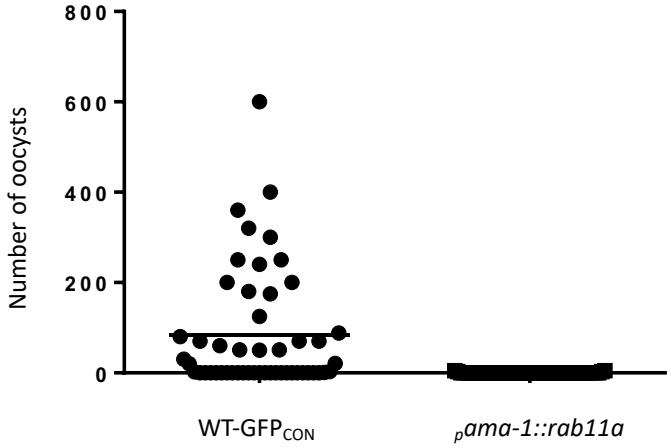
800
600
400
200
0
Number of oocysts
WT-GFP$_{CON}$
$_{p}$*ama-1::rab11a*

B

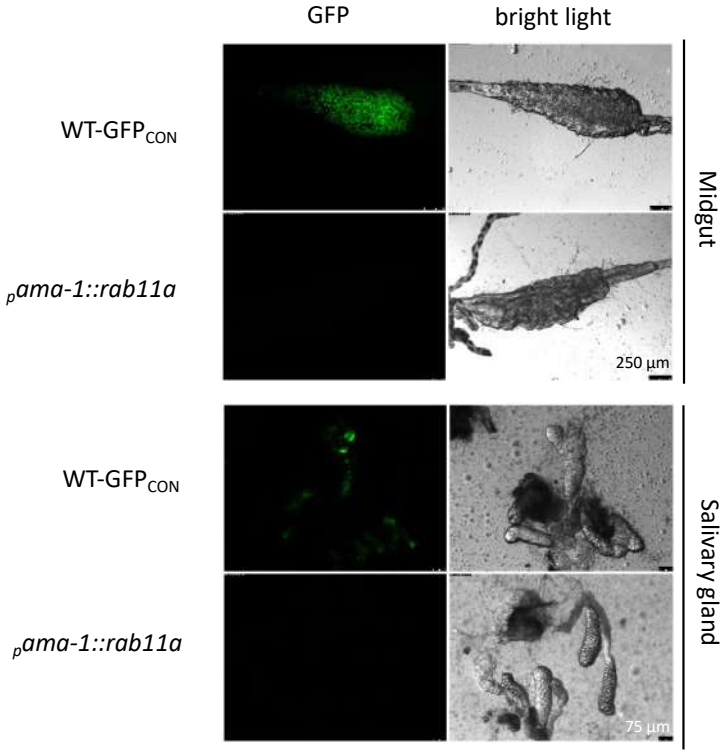
GFP
bright light
WT-GFP$_{CON}$
$_{p}$*ama-1::rab11a*
Midgut
250 µm
WT-GFP$_{CON}$
$_{p}$*ama-1::rab11a*
Salivary gland
75 µm

Figure S9

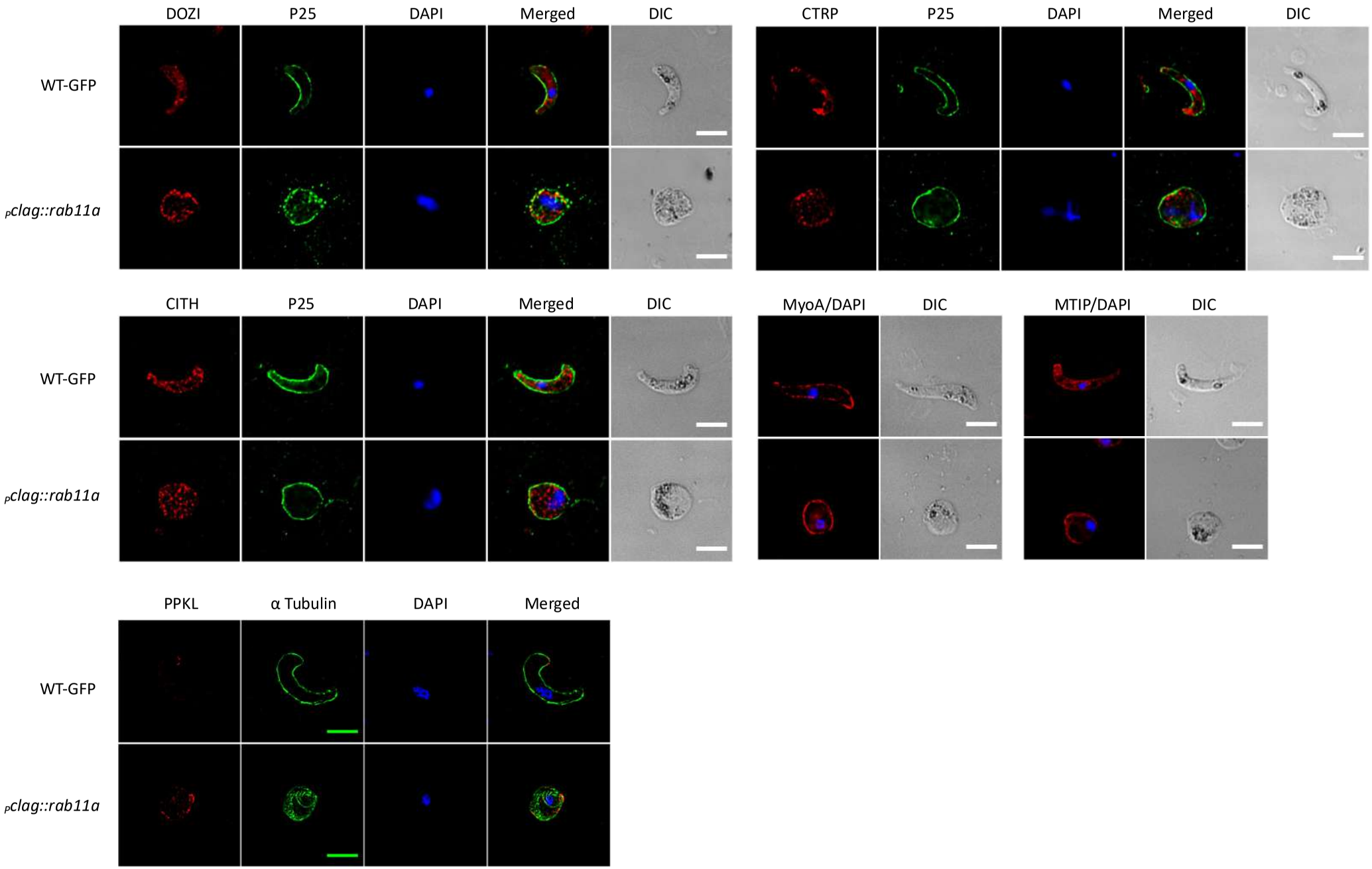
DOZI
P25
DAPI
Merged
DIC
CTRP
P25
DAPI
Merged
DIC
WT-GFP
pclag::rab11a
CITH
P25
DAPI
Merged
DIC
MyoA/DAPI
DIC
MTIP/DAPI
DIC
WT-GFP
pclag::rab11a
PPKL
α Tubulin
DAPI
Merged
WT-GFP
pclag::rab11a

Figure S10

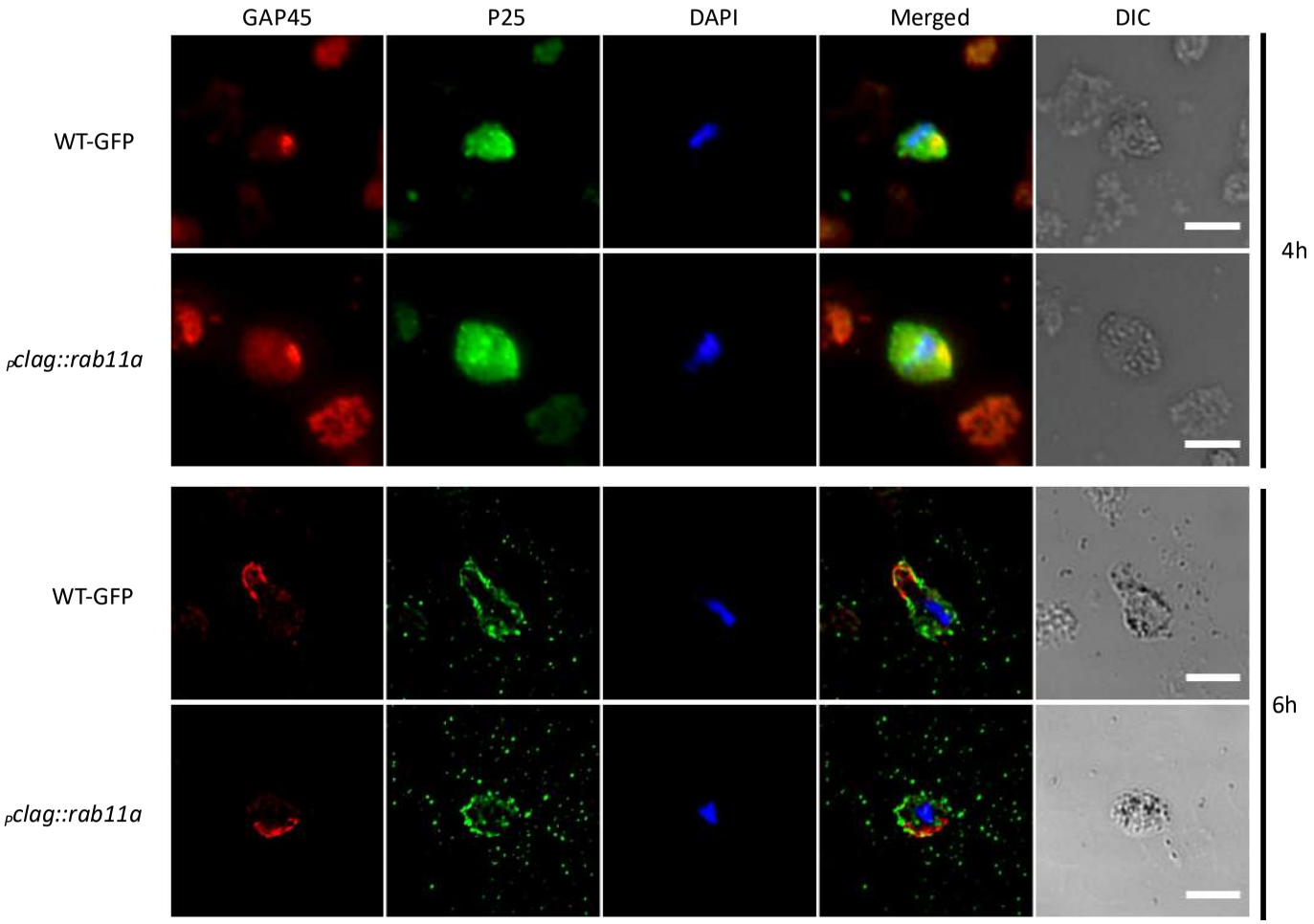
GAP45
P25
DAPI
Merged
DIC
WT-GFP
pclag::rab11a
4h
WT-GFP
pclag::rab11a
6h

Figure S11

significantly deregulated genes in WT gametocytes vs $_p$*clag::rab11A* gametocytes - 58

Upregulated -9

downregulated - 49

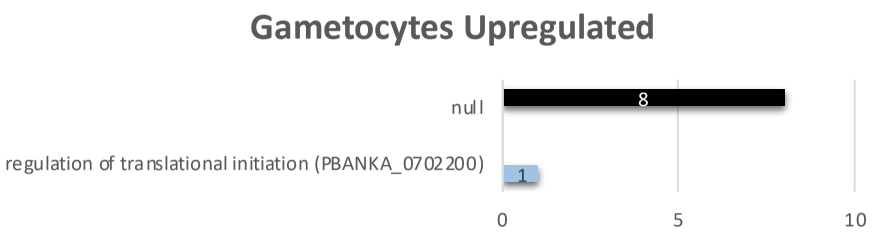

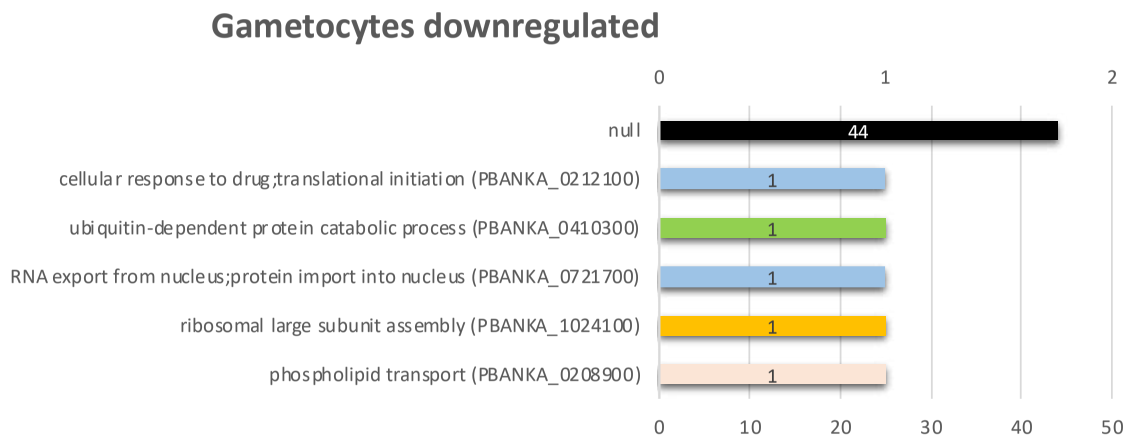

Figure S12 **Minimal overlap of DOZI KO, CITH KO and the *pclag::rab11a* gametocytes**

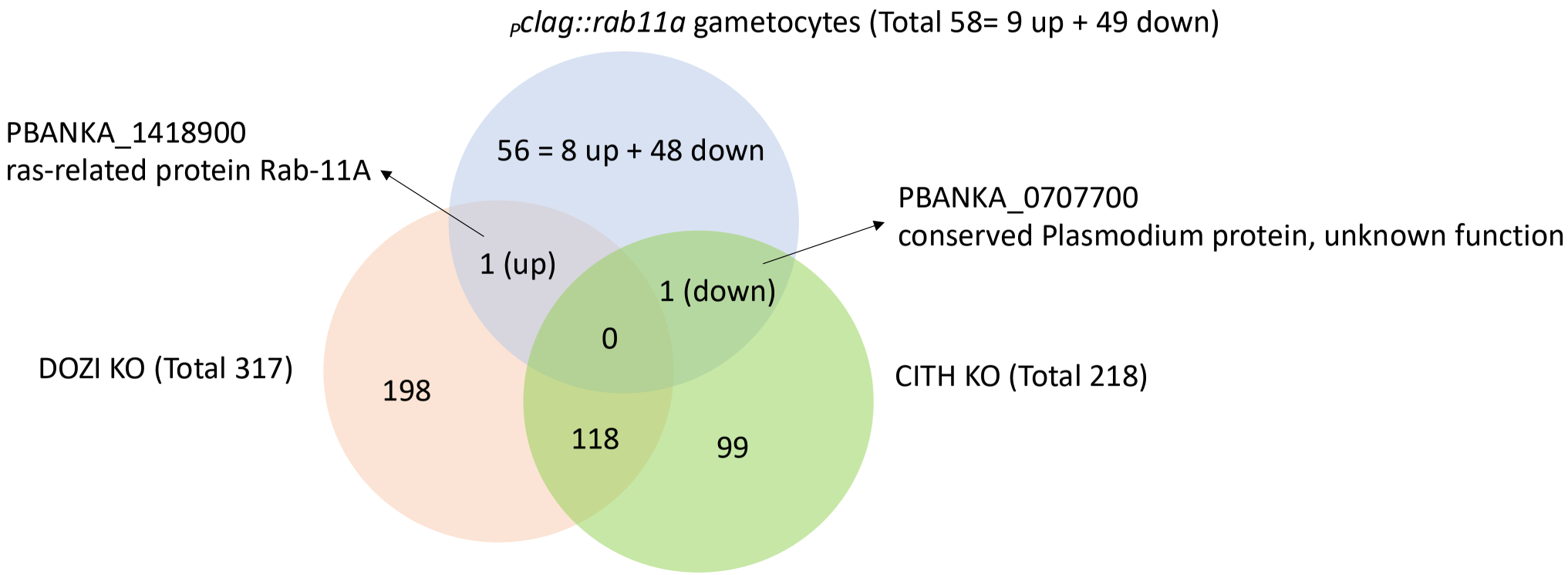

Figure S13

Deregulated genes in WT ookinete vs $_p$*clag::rab11A* spherical 24h ookinete - 116

Upregulated -84

downregulated - 32

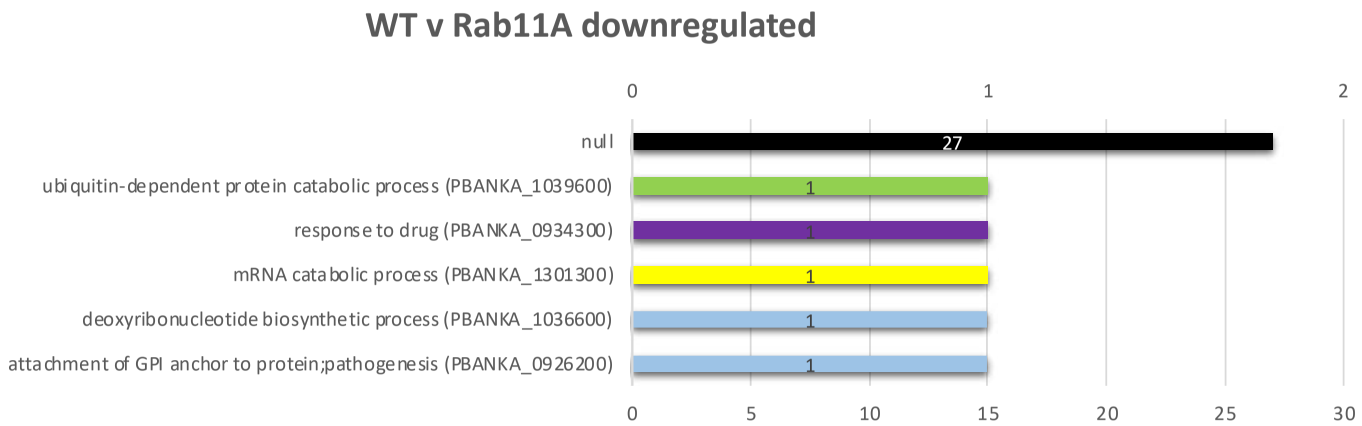

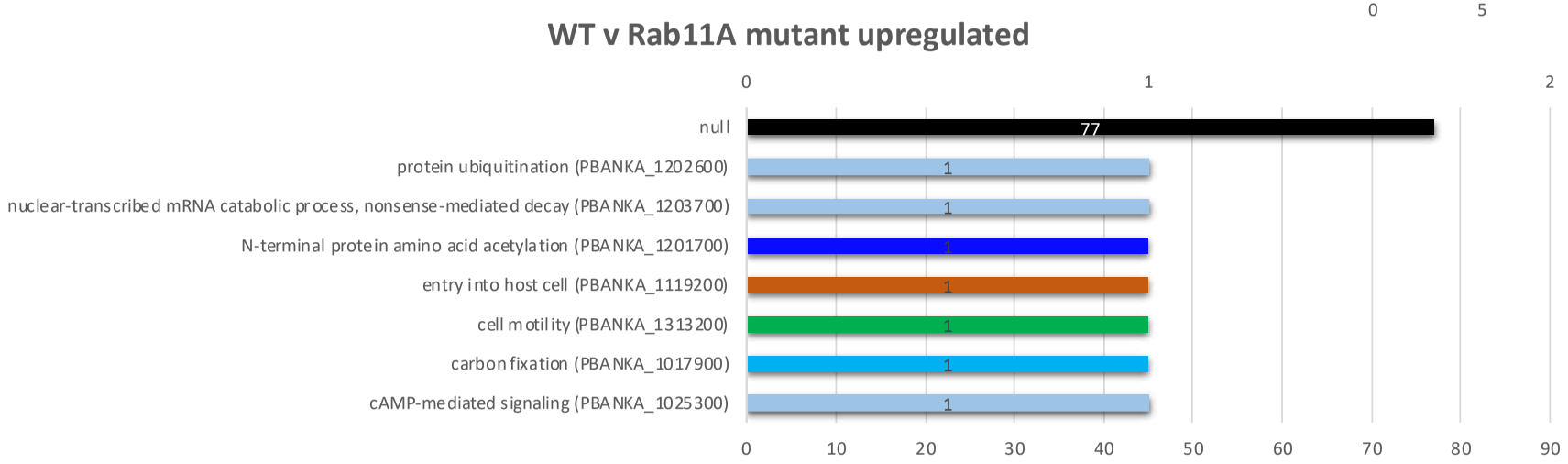

Supp Mov 1

Click here to access/download
Supporting Information
Patil et al Supp Mov 1.mov